

INTERIM REPORT

Accession No. _____

Report No. EGG-CAAD-5707

Contract Program or Project Title: Code Assessment and Applications Division

Subject of this Document: TRAC-PD2 Calculations of Semiscale Mod-1 Tests S-28-1 and S-28-10
(Steam Generator Tube Rupture Test Series)

Type of Document: Technical Report

Author(s): M. T. Hsu
C. D. Fletcher
A. C. Peterson

Date of Document: December 1981

Responsible NRC Individual and NRC Office or Division: F. Odar, NRC-RSR

This document was prepared primarily for preliminary or internal use. It has not received full review and approval. Since there may be substantive changes, this document should not be considered final.

EG&G Idaho, Inc.
Idaho Falls, Idaho 83415Prepared for the
U.S. Nuclear Regulatory Commission
Washington, D.C.
Under DOE Contract No. DE-AC07-76ID01570
NRC FIN No. A6047

INTERIM REPORT

NRC Research and/or Technical Assistance Report

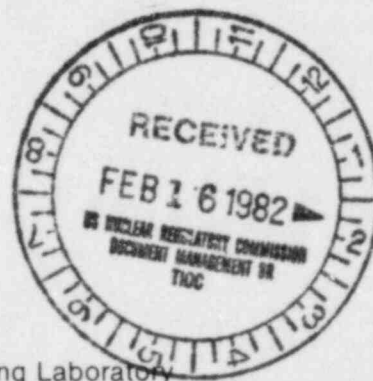
PAR

EGG-CAAD-5707

December 1981

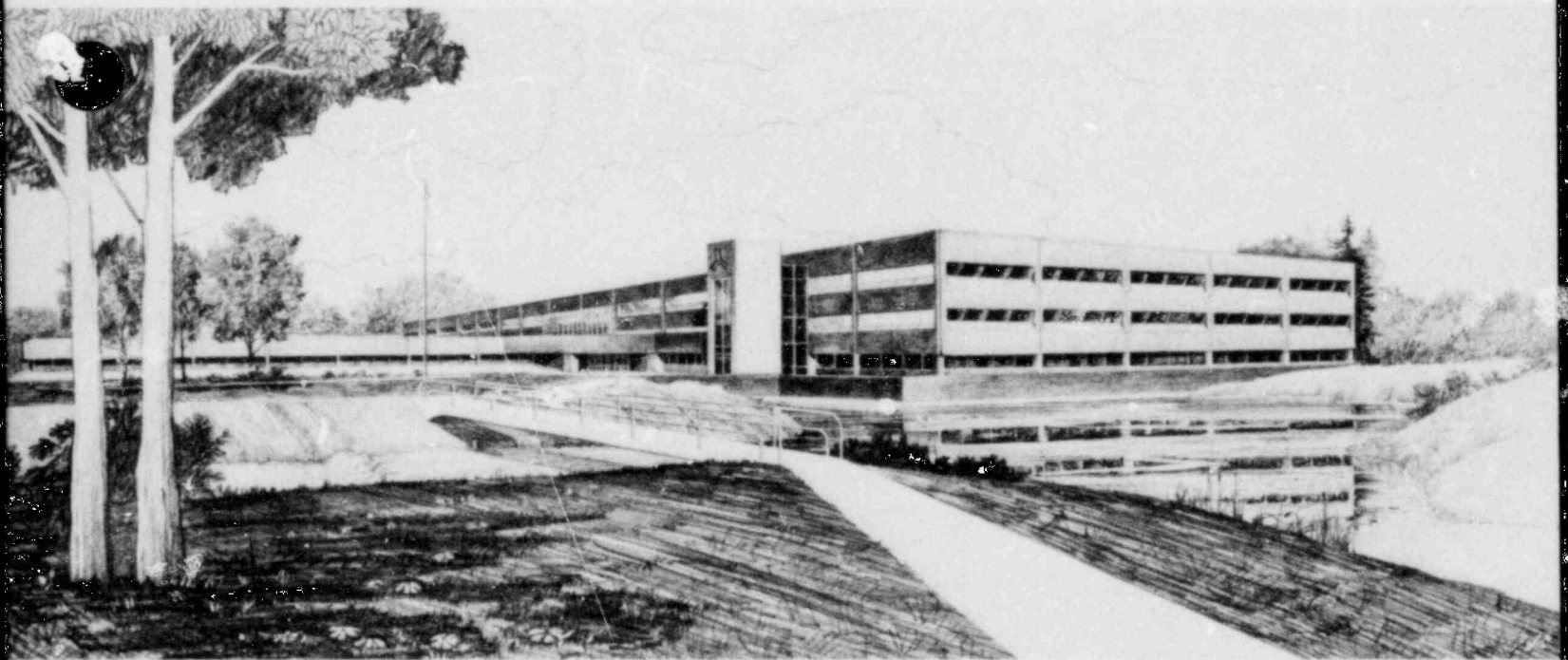
TRAC-PD2 CALCULATIONS OF SEMISCALE MOD-1
TESTS S-28-1 AND S-28-10
(STEAM GENERATOR TUBE RUPTURE TEST SERIES)

M. T. Hsu
C. D. Fletcher
A. C. Peterson



U.S. Department of Energy

Idaho Operations Office • Idaho National Engineering Laboratory



This is an informal report intended for use as a preliminary or working document

Prepared for the
U.S. Nuclear Regulatory Commission
Under DOE Contract No. DE-AC07-76ID01570
FIN No. A6047

 **EG&G** Idaho

ABSTRACT

Calculations were performed using the TRAC-PD2 computer code for Semiscale Mod-1 Test Series S-28 Large Break Loss-of-Coolant Accidents (LOCAs) concurrent with steam generator tube rupture. Calculations were made for Test S-28-1 and Test S-28-10 which represented a large and small number of ruptured steam generator tubes, respectively.

The calculated system hydraulic response and core thermal behavior were compared with experimental data. The capability of the TRAC-PD2 computer code to simulate the blowdown, refill, reflood and core quench phenomena was evaluated.

SUMMARY

Calculations of Semiscale Mod-1 steam generator tube rupture tests (Test Series S-28-1 and S-28-10) were performed using the TRAC-PD2 computer code. The main purpose of this analysis was to evaluate the capability of TRAC-PD2 to simulate the blowdown, rerail, reflood and core quench phenomena during a postulated large break Loss-of-Coolant Accident (LOCA) concurrent with the rupture of steam generator tubes.

The Semiscale Mod-1 system is a scaled model of a four-loop Pressurized Water Reactor (PWR) system. Semiscale Mod-1 consists of a pressure vessel with 40 electrically heated rods, an intact loop, a broken loop, pressure suppression system, and Emergency Core Cooling (ECC) system.

Tests S-28-1 and S-28-10 were performed to investigate the thermal-hydraulic response of the Semiscale Mod-1 system during a large break LOCA concurrent with steam generator tube ruptures. The specific objective was to determine the range of steam generator tube ruptures over which high peak cladding temperatures can occur. Test S-28-1 simulated the rupture of sixty tubes. Test S-28-10 simulated the rupture of twelve tubes.

The TRAC-PD2 calculations and test data were compared. In Test S-28-1, a preferential top down quench of the core caused by injection of liquid from the ruptured steam generator started at about 43.0 s, whereas, this type of quench occurred at 47.0 s in the calculation. The maximum rod temperatures calculated were on the low side of data. For Test S-28-10, there was not a top down quench of the core in either the data or the calculation. Instead, a bottomup quench occurred. In both comparisons, CHF prediction and temperature calculation were better in the lower and middle core than upper core. In the upper core region, CHF occurred in the data but was not calculated by the code and temperature comparisons were poor.

The calculations of the system hydraulic response followed the overall trend of data and the agreement between the data and the calculation were generally good.

CONTENTS

ABSTRACT.....	ii
SUMMARY	iii
1. INTRODUCTION	1
2. EXPERIMENT DESCRIPTION	3
2.1 Semiscale Mod-1 System	3
2.2 S-28 Series Steam Generator Tube Rupture Test Conditions	5
3. TRAC-PD2 MODEL	11
3.1 Nodalization Scheme	11
3.2 Code Options	11
3.3 Steady State and Transient Calculations	16
4. RESULTS	18
4.1 Test S-28-1 Rupture of Sixty Steam Generator Tubes	18
4.1.1 System Hydraulic Response	18
4.1.2 Core Thermal Behavior	28
4.2 Test S-28-10 Rupture of Twelve Steam Generator Tubes	40
4.2.1 System Hydraulic Response	40
4.2.2 Core Thermal Behavior	47
5. USER EXPERIENCE	59
6. CONCLUSIONS AND RECOMMENDATIONS	61
7. REFERENCES	63
APPENDIX A--ERROR ESTIMATES OF DATA IN TESTS S-28-1 AND S-28-10	64

FIGURES

1. Semiscale Mod-1 system isometric	4
2. Semiscale Mod-1 core-plan view with thermocouple locations	6

3.	Semiscale Mod-1 core axial power distribution showing ratio of local power to peak power	7
4.	Schematic of equipment simulating steam generator tube rupture in the Mod-1 system	7
5.	TRAC-PD2 nodalization diagram of Semiscale Mod-1 system	12
6.	TRAC-PD2 nodalization diagram of Semiscale Mod-1 vessel and break nozzle	13
7.	Comparison of the calculated and measured system pressure response for Test S-28-1	19
8.	Comparison of the calculated and measured broken loop cold leg mass flow for Test S-28-1	19
9.	Comparison of the calculated and measured intact loop accumulator discharge volumetric flow for Test S-28-1	21
10.	Comparison of the calculated and measured broken loop accumulator discharge volumetric flow for Test S-28-1	21
11.	Comparison of the calculated and measured intact loop hot leg mass flow for Test S-28-1	22
12.	Comparison of the calculated and measured intact loop cold leg mass flow for Test S-28-1	22
13.	Calculated void fraction in intact loop cold leg upstream of the ECC injection location for Test S-28-1	23
14.	Calculated void fraction in the intact loop cold leg at the ECC injection location for Test S-28-1	23
15.	Comparison of the calculated and measured core inlet mass flow for Test S-28-1	25
16.	Calculated liquid mass in downcomer for Test S-28-1	25
17.	Comparison of the calculated and measured intact loop cold leg density for Test S-28-1	26
18.	Comparison of the calculated and measured broken loop hot leg density for Test S-28-1	26
19.	Comparison of the calculated and measured broken loop fluid temperature for Test S-28-1	27
20.	Comparison of the calculated and measured lower plenum fluid temperature for Test S-28-1	27

21. Calculated liquid velocities and cell void fractions in vessel Level 16 at 49.24 s for Test S-28-1	29
22. Comparison of the calculated and measured rod cladding temperature at first level of core region for Test S-28-1	30
23. Comparison of the calculated and measured rod cladding temperature at second level of core region for Test S-28-1	30
24. Comparison of the calculated and measured rod cladding temperature at third level of core region for Test S-28-1	31
25. Comparison of the calculated and measured rod cladding temperature at fourth level of core region for Test S-28-1	31
26. Comparison of the calculated and measured rod cladding temperature at fifth level of core region for Test S-28-1	32
27. Comparison of the calculated and measured rod cladding temperature at sixth level of core region for Test S-28-1	32
28. Comparison of the calculated and measured rod cladding temperature at seventh level of core region for Test S-28-1	33
29. Comparison of the calculated and measured rod cladding temperature at eighth level of core region for Test S-28-1	33
30. Comparison of the calculated and measured rod cladding temperature at ninth level of core region for Test S-28-1	34
31. Comparison of the calculated and measured rod cladding temperature at tenth level of core region for Test S-28-1	34
32. Calculated cladding temperatures of average core heater rods at middle core elevation	39
33. Comparison of the calculated and measured system pressure response for Test S-28-10	42
34. Comparison of the calculated and measured broken loop cold leg mass flow for Test S-28-10	42

35.	Comparison of the calculated and measured intact loop accumulator discharge volumetric flow for Test S-28-10	44
36.	Comparison of the calculated and measured broken loop accumulator discharge volumetric flow for Test S-28-10	44
37.	Comparison of the calculated and measured intact loop hot leg mass flow for Test S-28-10	45
38.	Comparison of the calculated and measured intact loop cold leg mass flow for Test S-28-10	45
39.	Calculated void fraction in intact loop cold leg upstream of ECC injection location for Test S-28-10	46
40.	Comparison of the calculated and measured core inlet mass flow for Test S-28-10	46
41.	Comparison of the calculated and measured core inlet density for Test S-28-10	48
42.	Comparison of the calculated and measured intact loop cold leg density for Test S-28-10	48
43.	Comparison of the calculated and measured lower plenum fluid temperature for Test S-28-10	49
44.	Comparison of the calculated and measured rod cladding temperature at first level of core region for Test S-28-10	49
45.	Comparison of the calculated and measured rod cladding temperature at second level of core region for Test S-28-10	50
46.	Comparison of the calculated and measured rod cladding temperature at third level of core region for Test S-28-10	50
47.	Comparison of the calculated and measured rod cladding temperature at fourth level of core region for Test S-28-10	51
48.	Comparison of the calculated and measured rod cladding temperature at fifth level of core region for Test S-28-10	51
49.	Comparison of the calculated and measured rod cladding temperature at sixth level of core region for Test S-28-10	52

50. Comparison of the calculated and measured rod cladding temperature at seventh level of core region for Test S-28-10	52
51. Comparison of the calculated and measured rod cladding temperature at eighth level of core region for Test S-28-10	53
52. Calculated cladding temperatures of average core heater rods at mid-core elevation for Test S-28-10	58

TABLES

1. Tube rupture flow rates and rupture initiation times	8
2. Sequence of events for Tests S-28-1 and S-28-10	9
3. Conditions at blowdown initiation for Tests S-28-1 and S-28-10	10
4. Elevations of heated rod levels in TRAC-PD2 calculations	15
5. Maximum core temperature as a function of core levels for Test S-28-1	35
6. Maximum core temperature in each core region for Test S-28-1	36
7. Comparison of calculated and measured CHF for Test S-28-1	38
8. Quench time as a function of core elevation at core heater rod region four for Test S-28-1	41
9. Calculated quench time as a function of core elevation at core at core heater rod four for Test S-28-1	41
10. Quench time as a function of core elevation for Test S-28-10	54
11. Maximum temperature as a function of core elevation for Test S-28-10	56
12. Comparison of calculated and measured CHF for Test S-28-10	57
A-1. Measurements and their uncertainties	65

1. INTRODUCTION

This report describes TRAC-PD2 calculations of Semiscale Mod-1 steam generator tube rupture tests S-28-1 and S-28-10. The purpose of this study was to evaluate the capability of the TRAC-PD2 computer code to simulate the shutdown, refill, reflood, and core quench phenomena during a postulated large break Loss-of-Coolant Accident (LOCA) in a Pressurized Water Reactor (PWR) system concurrent with steam generator tube ruptures.

Tests S-28 were a series of steam generator tube rupture tests conducted on the Semiscale Mod-1 system. The specific objective of this test series was to determine the range of steam generator tube rupture over which high peak cladding temperatures occur. Two tests were analyzed in this study. Test S-28-1¹ represented a rupture of sixty tubes initiated 40 s after LOCA. Test S-28-10² represented a small rupture of twelve tubes initiated 60 s after LOCA.

The Semiscale Mod-1³ system is a scaled nonnuclear experimental facility with components representing the major features of a typical four-loop commercial PWR. It consists of a pressure vessel, an intact loop with pressurizer, steam generator and active pump, a broken loop with simulated steam generator and pump, and a rupture assembly with pressure suppression system. It also has an emergency core coolant system consisting of a high and low pressure injection system (HPIS and LPIS) and an accumulator for each loop. The core in the vessel has 40 electrically heated rods to simulate nuclear heating. For the steam generator tube rupture tests, the flow from the tube ruptures was simulated by the injection of liquid into the intact loop hot leg at a location just upstream of the steam generator inlet plenum. The injection was accomplished using a constant pressure accumulator with water at a temperature typical of a PWR steam generator secondary fluid.⁴

The Transient Reactor Analysis Code (TRAC)⁵ used in this study is an advanced best-estimate system computer program designed primarily for the analysis of a large break LOCA in a PWR. TRAC-PD2 is the latest publicly

released version. The main features of TRAC-PD2 include a three-dimensional representation of the pressure vessel, one-dimensional representation of piping and other components, a two-phase nonequilibrium model, flow-regime-dependent constitutive equations, reflood tracking capability for both bottom reflood and falling film quenching front, and a consistent treatment of the entire accident sequence including the generation of consistent initial conditions.

In the calculations, the steady state option was run for 70 s to reach initial conditions that were consistent with test initial conditions. After steady state was reached, transient calculations were performed. For Test S-28-1 the transient calculation ran for 60 s; for Test S-28-10 the calculation ran for 120 s. Each calculation was terminated before completing the entire transient because the calculations were running very slowly and it was judged that no significant additional information on the capabilities of TRAC-PD2 would be obtained in continuing the calculations.

This report documents comparisons between TRAC-PD2 calculations and test data. Section 2 of this report contains a description of the Semiscale Mod-1 test facility and Test S-28-1 and S-28-10 conditions. The TRAC-PD2 system model is discussed in Section 3. Comparisons of calculated results and measured data are presented in Section 4. The user experiences drawn from this study which will be helpful for future code application are presented in Section 5. Conclusions and recommendations are presented in Section 6.

2. EXPERIMENT DESCRIPTION

The Semiscale Mod-1 facility and S-28 series steam generator tube rupture test conditions are described in this section.

2.1 Semiscale Mod-1 System

The Semiscale Mod-1 system is a scaled model of a typical four-loop commercial PWR. Its main components are

1. A pressure vessel with simulated reactor internals, a downcomer, lower plenum, upper plenum, and heated core region.
2. 40 electrically heated rods in the core, of which four rods are unpowered to simulate the control rods.
3. An intact loop that is volume scaled to three loops of a PWR and contains a pressurizer, a tube-in-shell steam generator, and an active circulating pump.
4. A broken loop that is volume scaled to a single loop of a PWR and contains a simulated steam generator, simulated pump and rupture assemblies that consist of diaphragm rupture discs and converging-diverging blowdown nozzles to provide the desired break area.
5. A pressure suppression system that simulates the back pressure created by the containment building in a PWR.
6. An ECC injection system that interfaces with the intact and broken loop cold legs and includes a coolant injection accumulator and high pressure and low pressure injection systems.

Detailed descriptions of the system can be found in Reference 3. Figure 1 depicts the Semiscale Mod-1 system configuration.

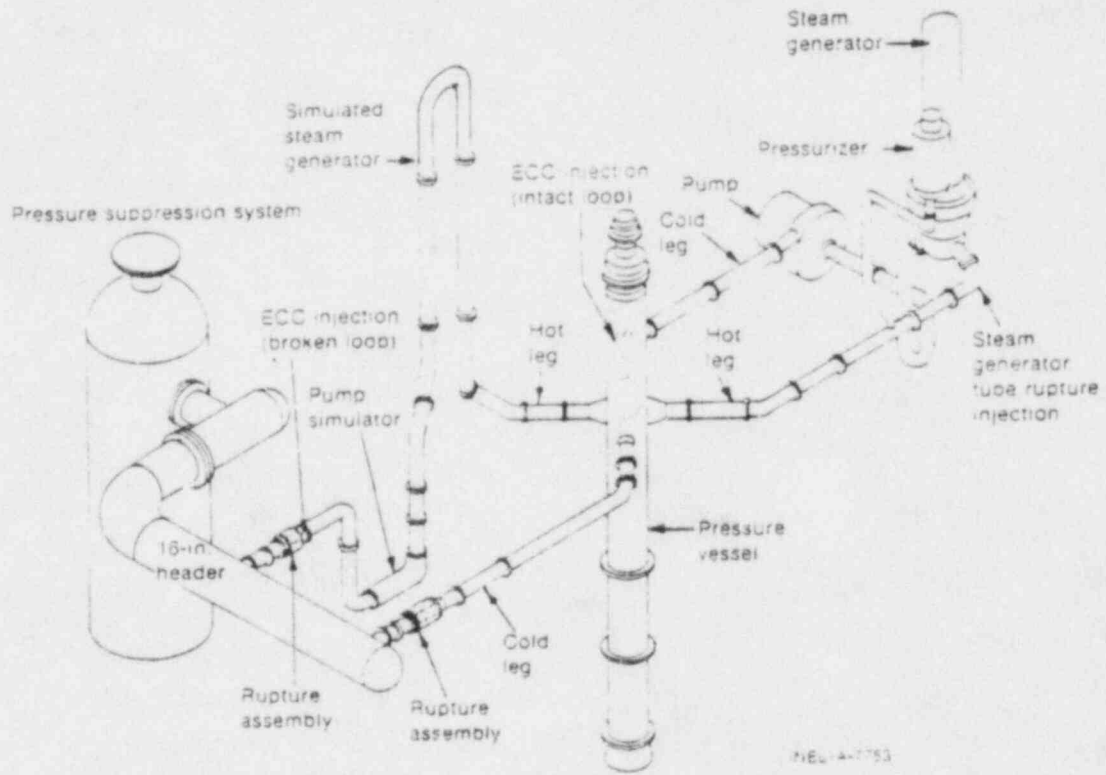


Figure 1. Semiscale mod-1 system isometric.

Figure 2 shows the Semiscale Mod-1 core configuration. It has 40 electrically heated rods, of which only 36 were powered. The heated length of the powered rods was 1.68 m with ten power steps providing a slightly bottom skewed axial power profile. The normalized axial power profile is illustrated in Figure 3. Of the 36 heated rods, three rods (Rods D-4, E-4, and E-5) were operated at a 5% higher peak power density than the remaining 33 heated rods to simulate the radial power profile near a control rod thimble in a PWR fuel assembly (peak power density of 39.7 kW/m for three high powered rods versus 37.7 kW/m for the remaining 33 rods). The four unpowered rods (Rods C-3, D-5, F-3, and F-6) simulated the effect of control rods guide tubes.

2.2 S-28 Series Steam Generator Tube Rupture Test Conditions

The 200% double-ended offset shear break in the cold leg of a PWR was simulated by connecting the cold legs to the pressure suppression tank.

For the steam generator tube rupture the secondary-to-primary flow due to the rupture of steam generator tubes was simulated by a controlled injection of liquid into the intact loop hot leg just upstream of the steam generator inlet plenum. The equipment arrangement required to simulate the secondary-to-primary flow is illustrated in Figure 4.

The simulated constant secondary-to-primary flow rate was maintained during the injection period for each test, but was changed between tests to represent different numbers of ruptured steam generator tubes. Table 1 lists the injection rate and injection time interval for Tests S-28-1 and S-28-10.

To simulate the change in heat transfer in the intact loop steam generator, secondary fluid was discharged to the atmosphere at a rate equivalent to the rate of the injected tube rupture flow.

The sequence of operating events for Tests S-28-1 and Test S-28-10 is listed in Table 2. The initial and boundary conditions are shown in Table 3. Appendix A contains an estimate of the measurement uncertainties.

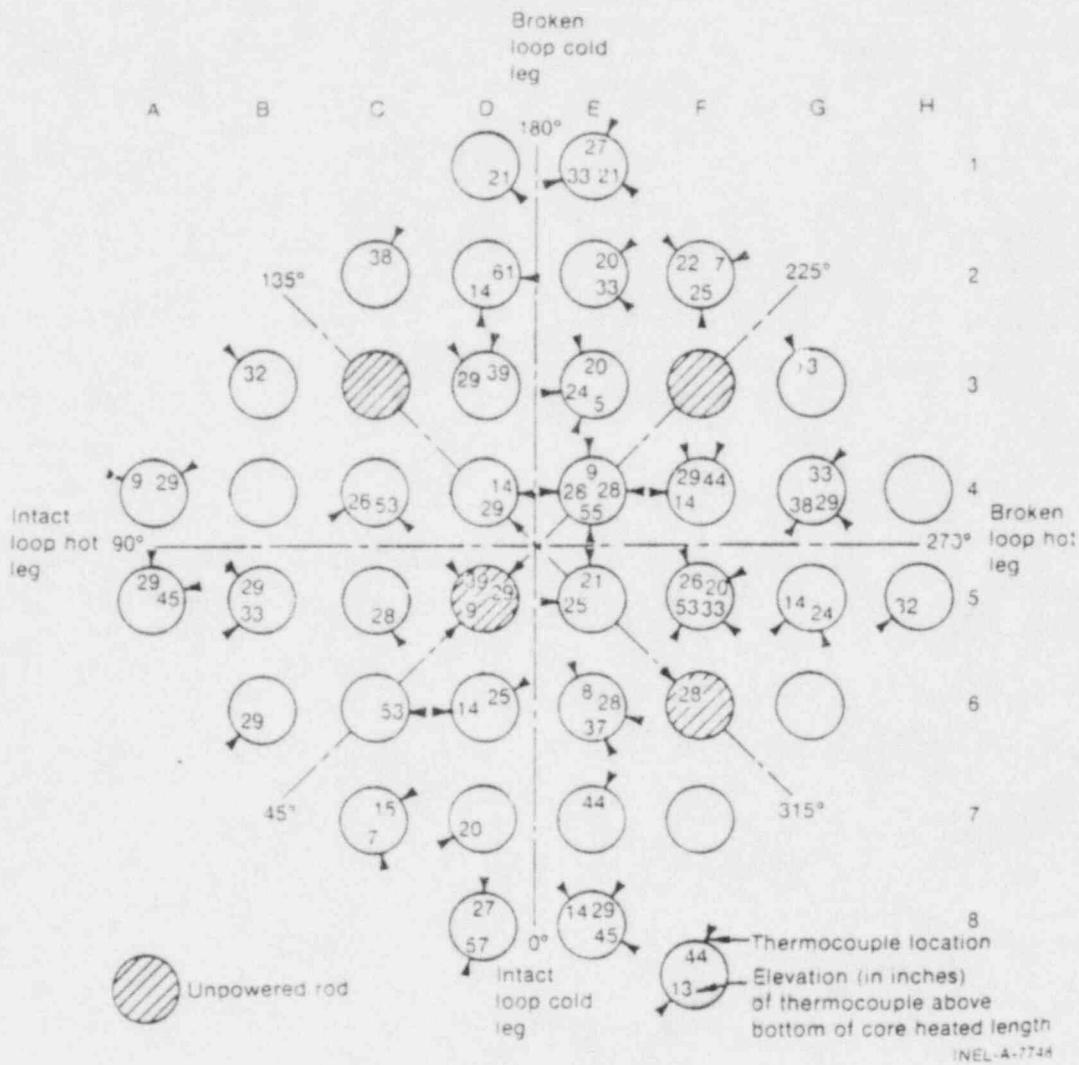


Figure 2. Semiscale Mod-1 core-plan view with thermocouple locations.

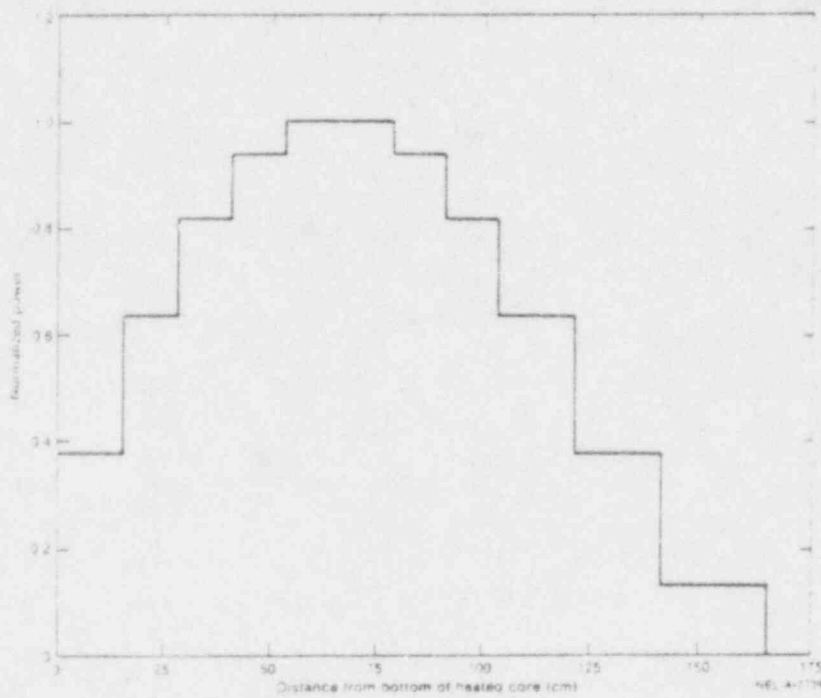


Figure 3. Semiscale Mod-1 core axial power distribution showing ratio of local power to peak power.

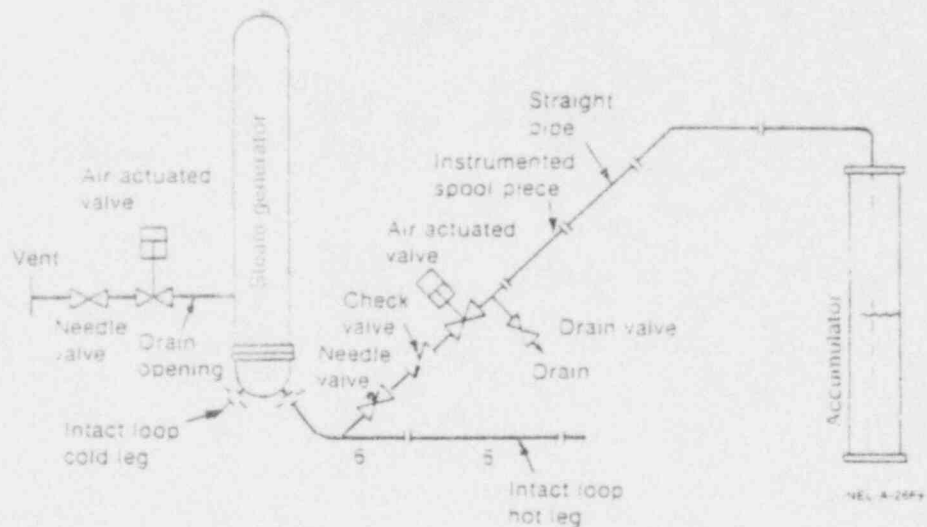


Figure 4. Schematic of equipment simulating steam generator tube rupture in the Mod-1 system.

TABLE 1. TUBE RUPTURE FLOW RATES AND RUPTURE OCCURRENCE TIMES

Test	Number of Steam Generator Tube Ruptures	Steam Generator Tube Rupture Flow Rate (kg/s)	Steam Generator Tube Rupture Flow Initiated (s)	Steam Generator Tube Rupture Flow Stopped (s)
S-28-1	60	0.544	40	240
S-28-10	12	0.109	60	640

TABLE 2. SEQUENCE OF EVENTS FOR TESTS S-28-1 and S-28-10

Event	Time Relative to Rupture (s)	
	Test S-28-1	Test S-28-10
Bypass lines valved out of system	-2.5	-2.5
Blowdown initiated	0	0
Pump power reduced	0	0
High pressure injection system pumps started	0	0
ECC accumulators valved in	0	0
Steam generator feedwater and discharge valves closed	1.0	1.0
Core power decay transient started	3.65	2.7
Low pressure injection system pumps started	28.0	26.0
Core power tripped off	640.0	645.0

TABLE 3. CONDITIONS AT BLOWDOWN INITIATION FOR TESTS S-28-1 AND S-28-10

	<u>Test S-28-1</u>	<u>Test S-28-10</u>
	<u>Measured</u>	<u>Measured</u>
Core power (MW)	1.391	1.42
Intact loop cold leg (K) temperature	557.0	556.0
Hot leg to cold leg temperature differential (K)	36.6	37.7
Pressurizer pressure (KPa)	15,767.0	15,703.0
Steam generator feedwater temperature (K)	480.0	480.0
Pressure suppression tank pressure (KPa)	241.0	244.0
Pressure suppression tank water temperature (K)	288.0	285.0

3. TRAC-PD2 MODEL

The TRAC-PD2 nodalization scheme, the user-selected code options, the initial and boundary conditions, and the sequence of test events used in the calculation are described in this section.

3.1 Nodalization Scheme

The nodalization scheme used in this study is based on the model developed in the analysis of Semiscale Mod-1 LOCE S-04-6.⁶ Figure 5 depicts the complete system nodalization except for the vessel and break which are shown in Figure 6. In total the entire model consisted of 26 components, 27 junctions and 270 computational cells.

The major features of the model were:

1. The intact loop was represented by two tee components in the hot leg, a steam generator, a pipe, a pump, and one tee component in the cold leg. A pressurizer was connected to the first tee component in the hot leg. The fill component simulating the injection of secondary side steam generator liquid to primary side was connected to the secondary side of a tee in the hot leg. The steam generator secondary side included the downcomer and steam separator. The fill components connected to the downcomer had a positive inlet flow during steady state calculations simulating the feedwater inlet flow, and negative flow during transient calculation simulating the drainage of secondary side steam generator liquid. A valve was added to the outlet side of the steam separator which was tripped to shut off the steam outlet flow completely.
2. The broken loop hot leg was modeled by a tee component and break.
3. The broken loop cold leg was represented by a pipe and break which connected to the pressure suppression tank.

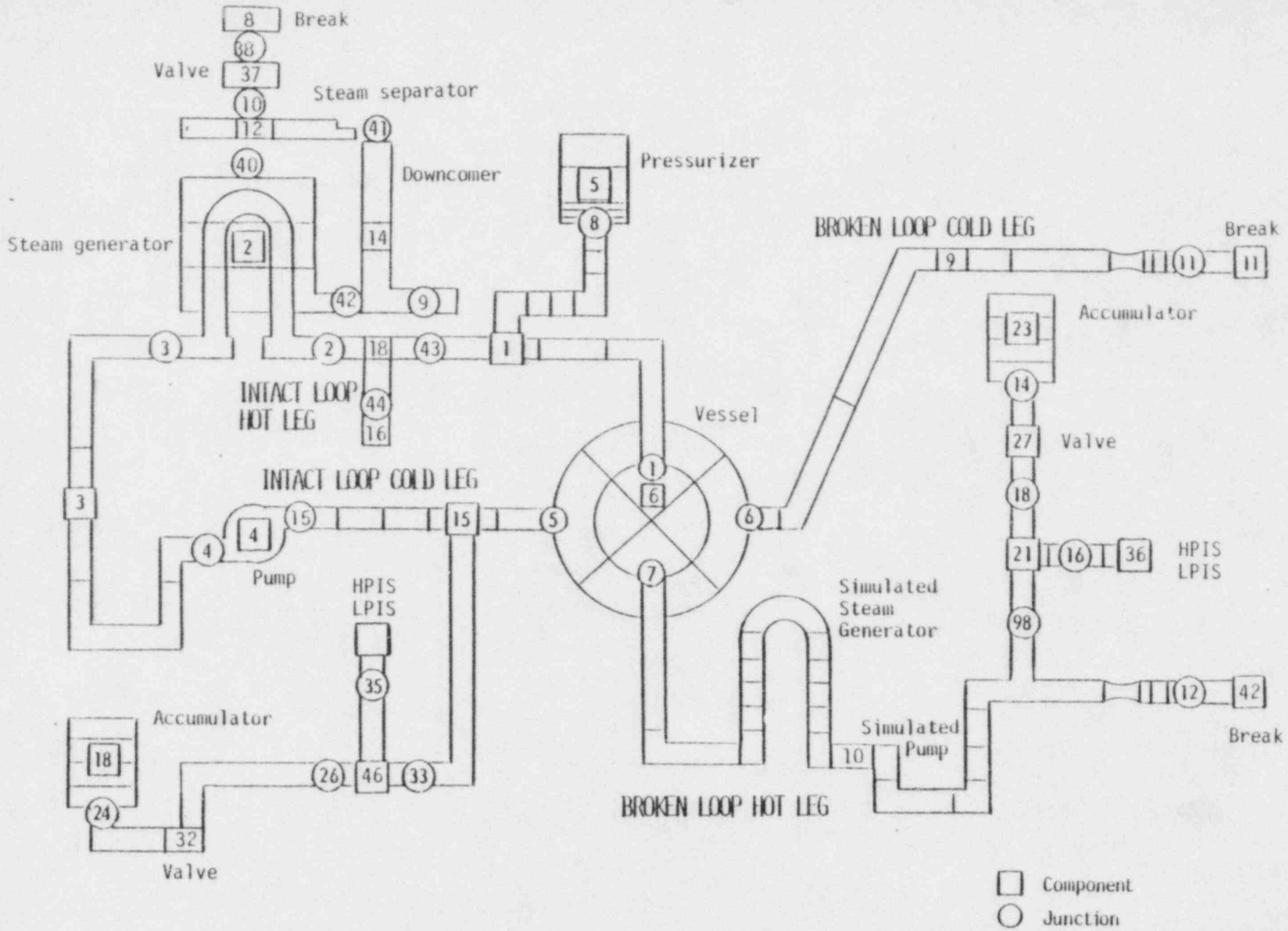


Figure 5. TRAC-PD2 nodalization diagram of Semiscale Mod-1 system.

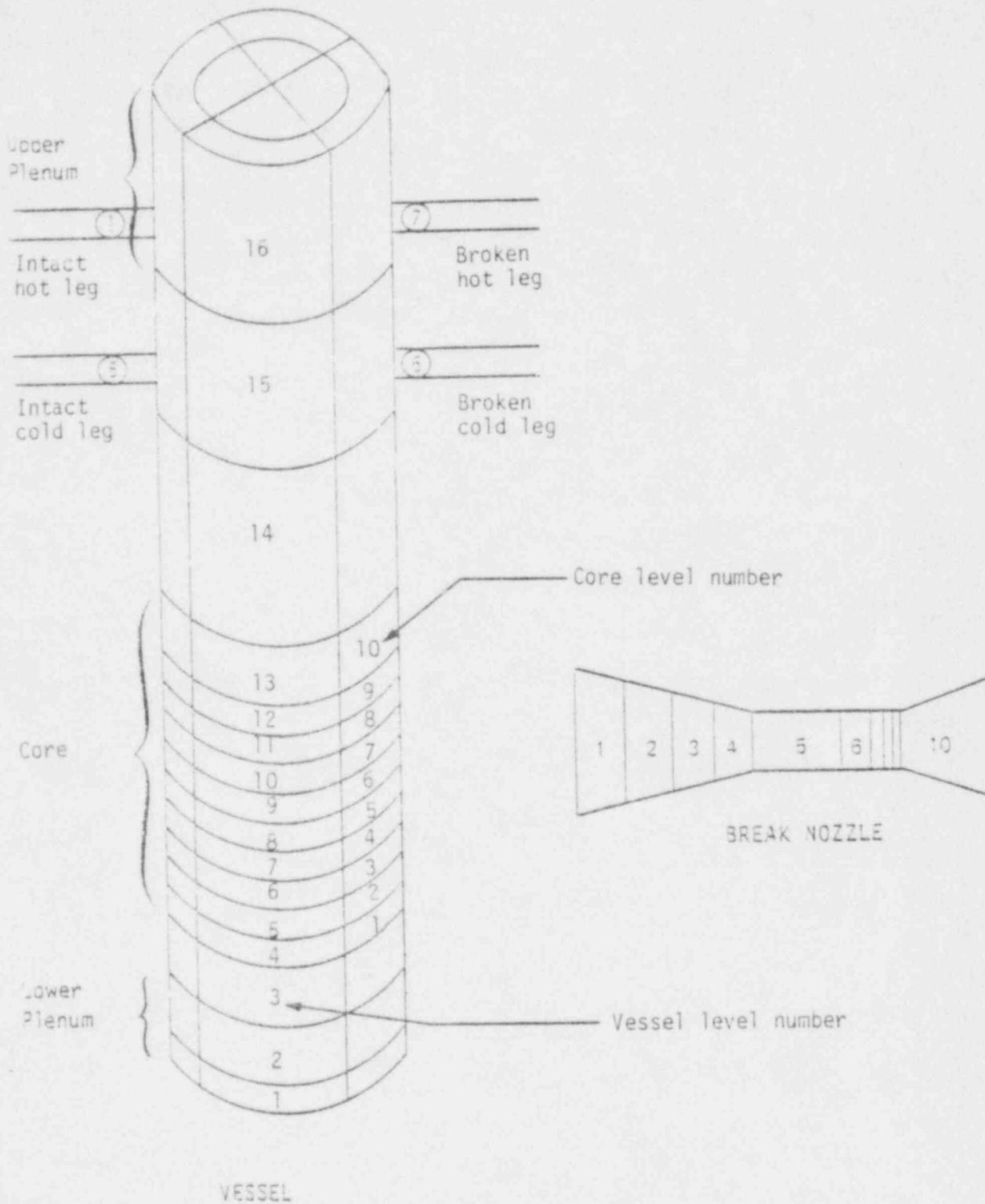


Figure 6. TRAC-PD2 nodalization diagram of Semiscale Mod-1 vessel and break nozzle.

4. The pressure suppression system was represented by break components with constant pressure.
5. The break nozzles were finely nodalized to calculate the break flow accurately.
6. The intact and broken loop ECC systems were each represented by an accumulator component, a valve component with the check valve option, single fill component representing the combination of the high pressure injection system (HPIS) and the low pressure injection system (LPIS). The fill component used the velocity versus pressure option to simulate the actual pump performance.
7. The vessel contained 16 axial levels with each axial level containing two radial segments and four azimuthal segments. This nodalization had 128 cells in the vessel. The lower plenum was represented by the first two axial levels and the upper plenum was represented by the last axial levels.
8. The active heated rods were represented by 10 axial levels and were modeled from Level 4 to Level 13. The elevations of each heated rod level were listed in Table 4. Each rod level corresponded to a power step in the slightly bottom-skewed axial power profile. Each heated rod had 10 radial heat transfer nodes.

3.2 Code Options

The S-28 steam generator tube rupture tests were conducted according to preset power versus time data, consequently, the core-power versus time option (IRPOP=7) was used in the calculations. The pump speed versus time option was used in the pump component since the pump coastdown option was found to produce a considerably retarded coastdown rate.⁶

The friction factor correlation option (input parameter NFF) and hydrodynamics numerical scheme option (input parameter IHYDRO) are two major user-selected code options in this calculation. Based on

TABLE 4. ELEVATIONS OF THE HEATED ROD LEVELS IN THE TRAC-PD2 CALCULATIONS

<u>Heated Rod Level</u>	<u>Elevation (m)</u>
1	0.0 to 0.1518
2	0.1518 to 0.2798
3	0.2798 to 0.4068
4	0.4068 to 0.5338
5	0.5338 to 0.7878
6	0.7878 to 0.9148
7	0.9148 to 1.0418
8	1.0418 to 1.2188
9	1.2188 to 1.4228
10	1.4228 to 1.67

recommendations from Reference 7, the annular flow correlation (NFF=4) was used for all components except the pressurizer and steam generator. For these two components, the homogenous flow correlation (NFF=1) was used as recommended by the TRAC User's Manual. In the numerical scheme selection, the partially implicit numerical hydrodynamics option (IHYDRO=0) was used throughout the system except at the secondary side of those components in the intact loop connecting the pressurizer and ECC system and the entire broken loop where fully implicit hydrodynamics option (IHDR0=1) was used exclusively. The fully implicit option is recommended to be used at locations where a rapid transient response is expected to occur.⁵

At all junctions, added friction was included to account for losses due to area changes, bends, tees, and instrumentation. Added friction was also included as experimentally determined for the pressurizer surge line, the accumulator lines, the steam generator, the simulated steam generator and pump, and the core to upper plenum region.

3.3 Steady State and Transient Calculation

Prior to the transient calculation, the steady state option of TRAC-PD2 was run. The broken loop components and ECC system were replaced by fill components with zero inlet flow as boundary conditions.

Steady state conditions could not be reached without changing the steam generator feed water mass flow rate from the experimental value of 0.7 kg/s to 4.45 kg/s, and changing the pump speed from data of 2000 rpm to 2400 rpm. Without these changes, the liquid mass at the secondary side of the steam generator was depleting and the temperature differential across the vessel would not agree with the data. With these changes, the calculated steady state temperature in the hot leg was within 1.1 K of the data and the calculated system pressure was within 1% of the measured pressure.

In the transient calculations, the entire system shown in Figure 5 was used. The inclusion of the broken loop and ECC system were to simulate the LOCA and operating events as described in Table 2. Also, fill Components 7

and 16 were used to simulate the injection and drainage of steam generator liquid during the tube rupture. For Test S-28-1, the tube rupture started at 40 s. For Test S-28-10, the tube rupture started at 60 s.

4. RESULTS

The calculated results of Tests S-28-1 and S-28-10 are analyzed in this section. The overall system hydraulic response and core thermal response are discussed.

4.1 Test S-28-1 Rupture of Sixty Steam Generator Tubes

In this section, the TRAC-PD2 calculations for the large number of ruptured steam generator tubes (Test S-28-1) are compared with experimental data. The parameters examined are pressure, volumetric flow, mass flow, density, system fluid temperatures and core temperatures. Results of the calculation are stored on Tape A46257; the graphic file is stored on Tape A50749.

The calculation was terminated after 60 s of the transient because the calculation was running very slowly and it did not appear that additional information on the capabilities of TRAC-PD2 would be obtained by continuing the calculation.

4.1.1 System Hydraulic Response

Figure 7 shows a comparison of the measured and calculated system pressure. The calculated pressure decreased slower than data for the first 2 s then faster than data until about 14 s.

A comparison of the calculated and measured broken loop cold leg mass flow rates shown in Figure 8, indicates the calculated flow was smaller than measured over the first 2 s and larger than measured until 14 s. These differences in the break mass flow caused the differences in the pressure responses. The measured break flow was established almost instantly whereas the calculated break flow required approximately 1 s to reach the maximum value. Between 2 and 14 s the higher calculated break flow resulted in a faster calculated depressurization rate. After 14 s the break flows agreed well and, as a result, the depressurization rates after 14 s agreed closely.

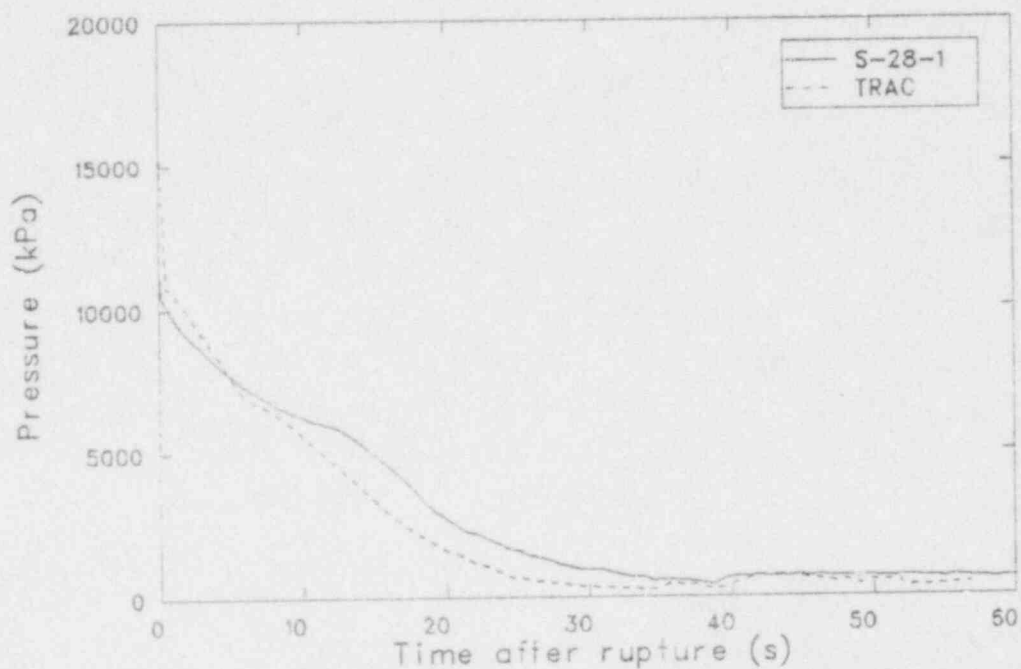


Figure 7. Comparison of the calculated and measured system pressure response for Test S-28-1.

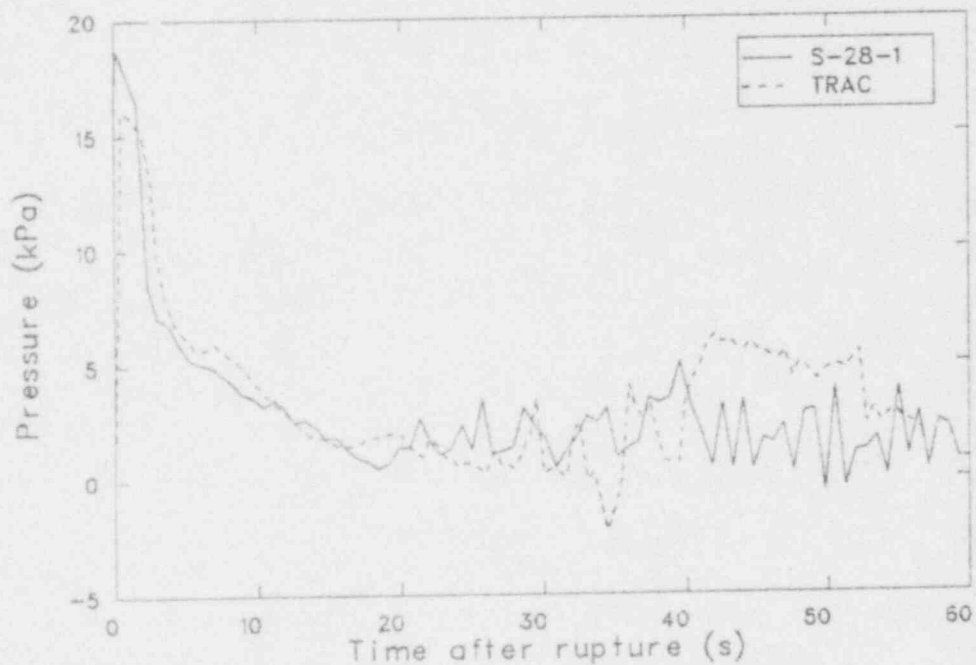


Figure 8. Comparison of the calculated and measured broken loop cold leg mass flow for Test S-28-1.

The consequence of the faster calculated depressurization was an earlier initiation of the ECC systems in the calculation. Figure 9 shows a comparison of the intact loop accumulator volumetric discharge rates. The accumulator flow was initiated at 14 s in the calculation and at 16.4 s in the experiment. The calculated flow developed to a higher level because the calculated primary pressure was below measured (Figure 7). As a result of earlier initiation and higher discharge rate, the modeled accumulator emptied early. A discharge of gas occurred at 48 s and the accumulator was empty at 55 s.

In the broken loop the initial accumulator liquid mass did not agree with the experiment. The model included 33.4 kg, whereas, the experiment included 16.42 kg of subcooled liquid in the broken loop accumulator. As a result, the accumulator in the test was depleted of liquid at 29 s and was nearly empty of gas at 60 s as shown in Figure 10. The calculation, because of the higher initial accumulator liquid mass, did not indicate a liquid depletion. This difference should not adversely affect the overall calculation results since the excess liquid was expelled through the break as evidence between 40 and 50 s in Figure 8 and should not significantly effect the overall results of the calculation.

The intact loop mass flow comparison is shown in Figure 11. Between 15 and 40 s the calculated flow was positive, whereas, the measured flow was negative. After 40 s, the time of the steam generator tube rupture, the calculated flow became negative. In the intact cold leg the comparison of mass flow rates was generally good as shown in Figure 12 with both calculated and measured data oscillating after 24 s. At 24 s, the calculational cell upstream of the ECC injection location started undergoing rapid changes in void fraction as shown in Figure 13, whereas, the cell at the injection location was liquid filled as shown in Figure 14. These figures indicate that at 24 s the accumulator fluid had filled all volumes downstream of the cold leg injection location and was starting to fill the cold leg in a direction toward the pump. During this process steam was being condensed in the cold leg which caused the calculation of a positive hot leg flow as shown in Figure 11. When the

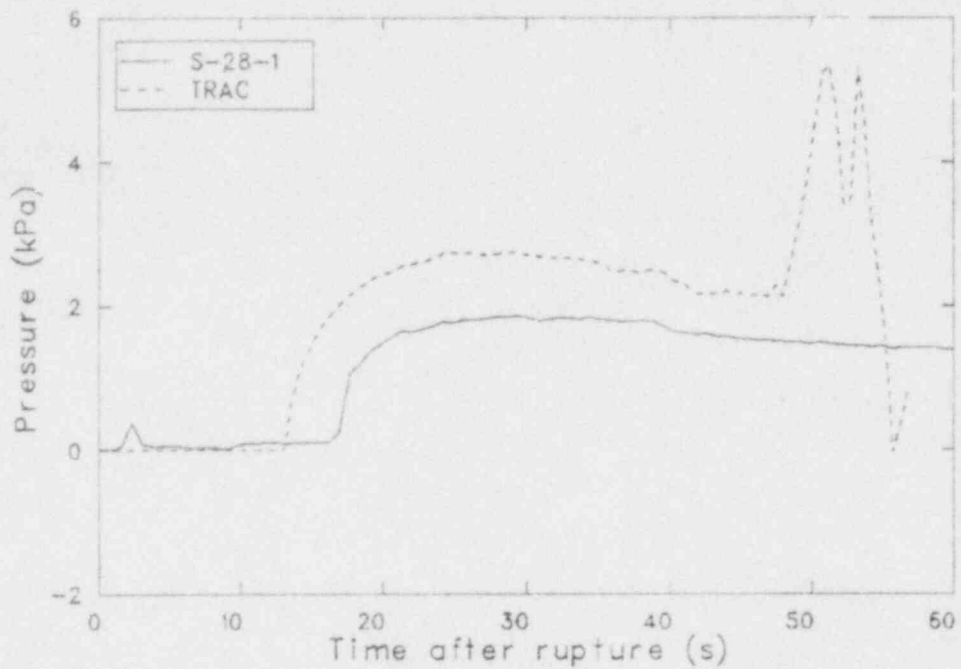


Figure 9. Comparison of the calculated and measured intact loop accumulator discharge volumetric flow for Test S-28-1.

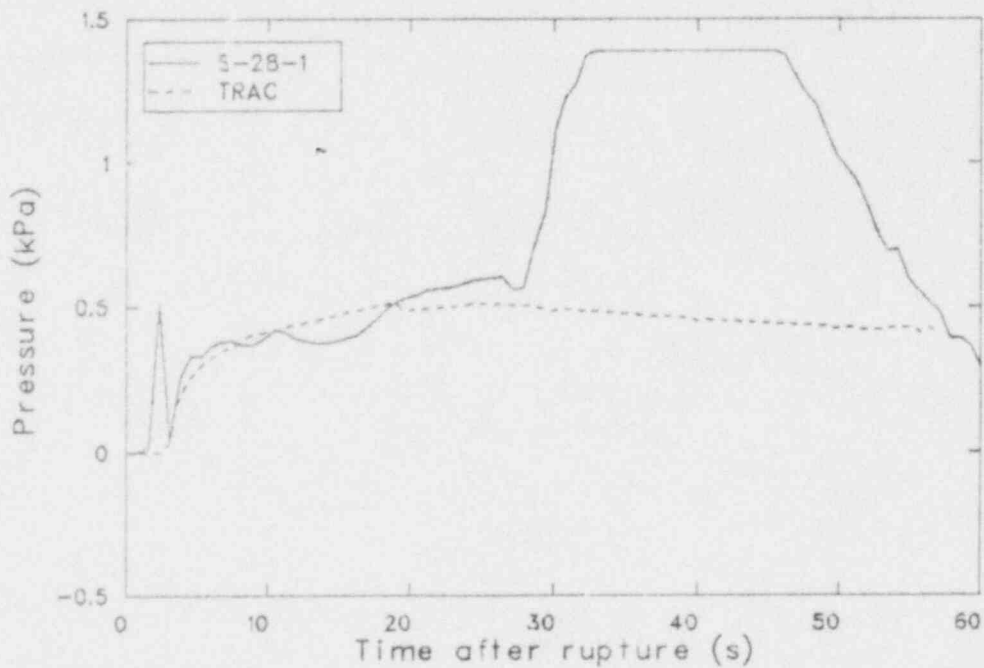


Figure 10. Comparison of the calculated and measured broken loop accumulator discharge volumetric flow for Test S-28-1.

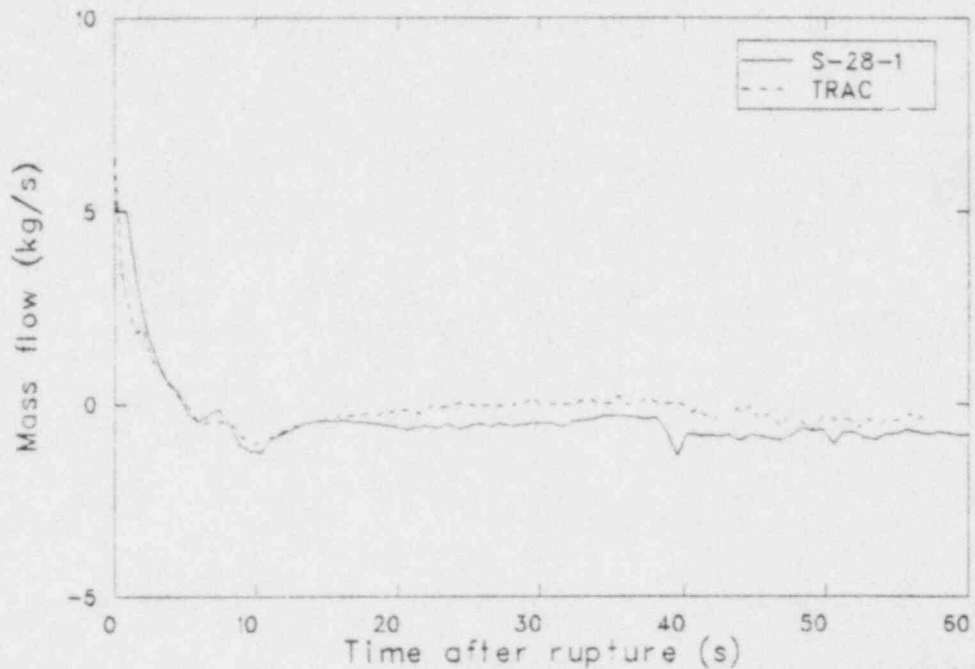


Figure 11. Comparison of the calculated and measured intact loop hot leg mass flow for Test S-28-1.

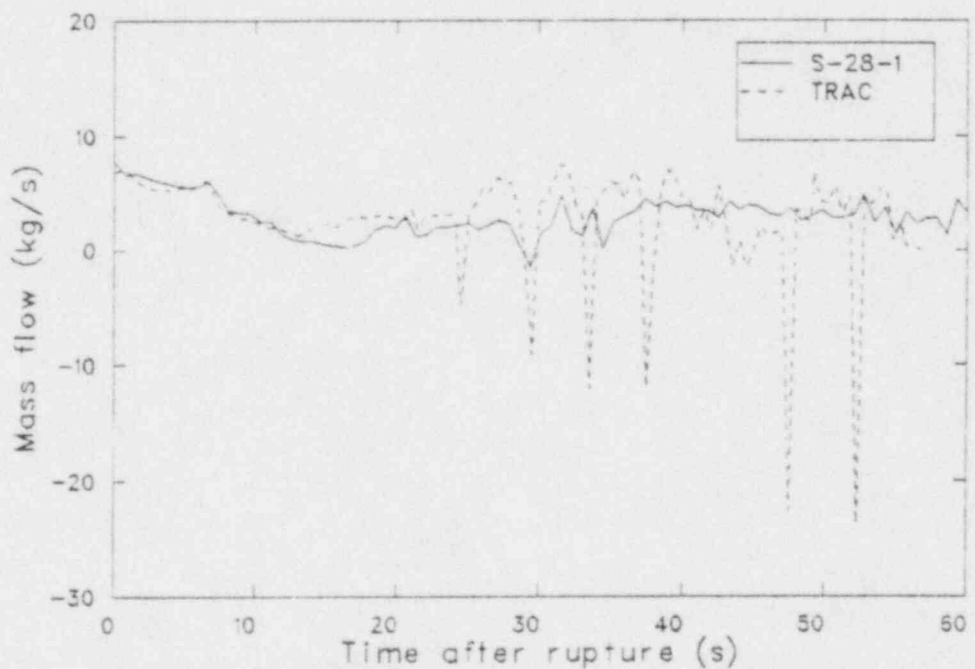


Figure 12. Comparison of the calculated and measured intact loop cold leg mass flow for Test S-28-1.

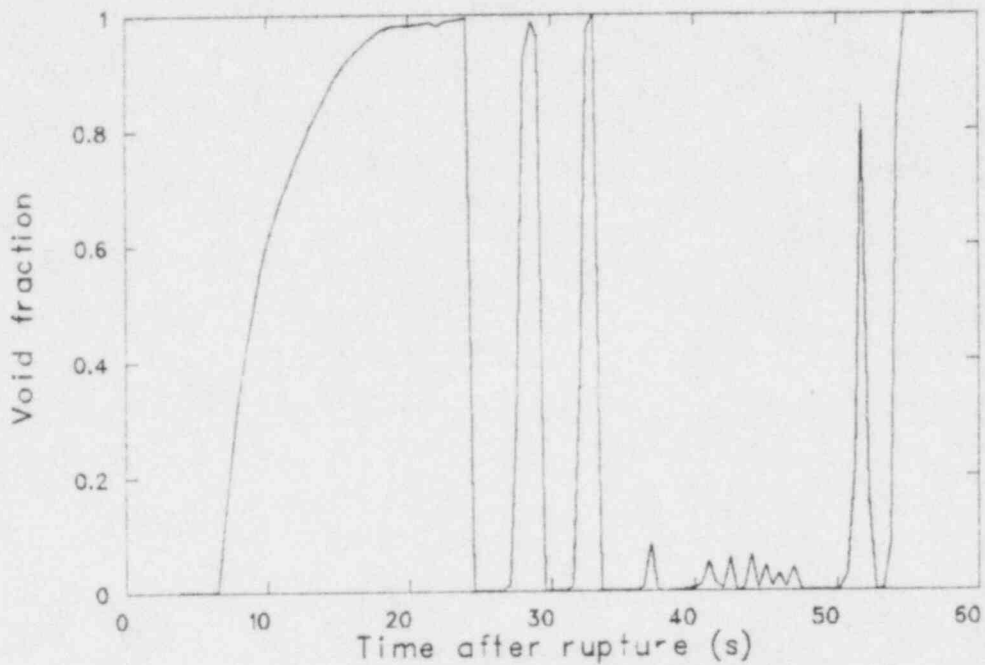


Figure 13. Calculated void fraction in intact loop cold leg upstream of the ECC injection location for Test S-28-1.

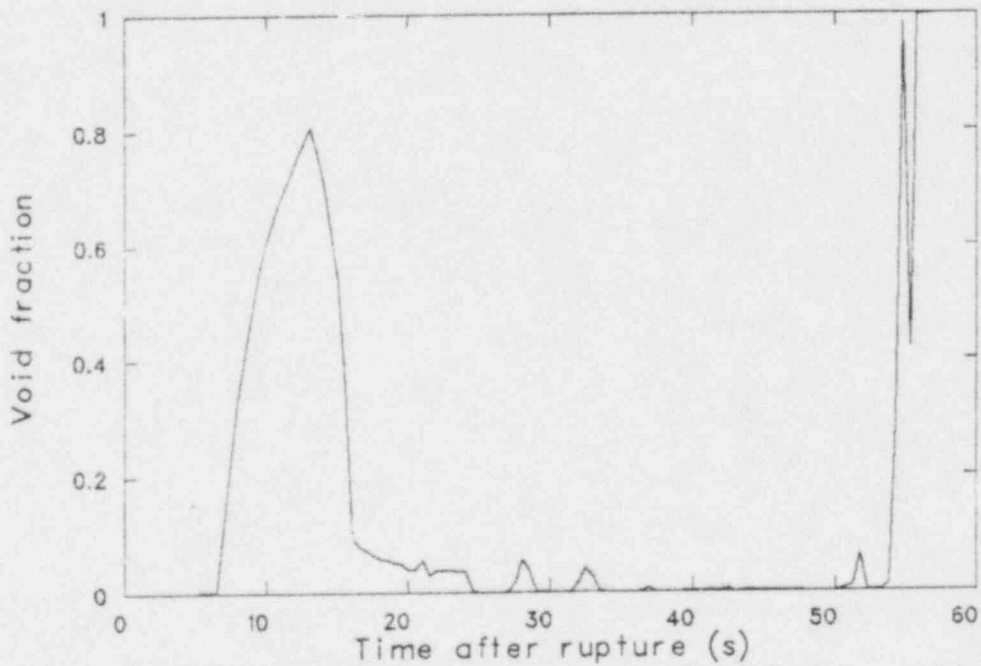


Figure 14. Calculated void fraction for the intact loop cold leg at the ECC injection location for Test S-28-1.

injected liquid reached the pump, the pump head increased rapidly, forcing the liquid back toward the vessel and caused the oscillations shown in Figures 12 and 13.

It appears that the calculated condensation rates in the cold leg were excessive thus causing both the calculation of a positive hot leg flow as shown in Figure 11 and the large magnitude of the oscillations shown in Figure 12.

Figure 15 shows a comparison of the calculated and measured core inlet mass flow. Reflood did not occur within 60 s in either the experiment or calculation. The flow surges in the calculation at about 38 s were a result of the condensation induced oscillations in the intact loop cold leg.

The calculated downcomer liquid mass is shown in Figure 16. The mass initially decreased as a result of the break flow then increased following the initiation of accumulator flow. The oscillations between 24 and 35 s resulted from the cold leg oscillations previously discussed and from steam generation in the core. After the steam generator tube ruptures at 40 s and the intact loop accumulator was emptied, the level in the downcomer decreased again.

A comparison of calculated and measured intact loop cold leg density is shown in Figure 17. The cold leg refilled with liquid about 2.5 s earlier in the calculation than measured because of the initiation of earlier accumulator flow. A comparison of the calculated and measured broken loop hot leg density, shown in Figure 18, illustrates good agreement occurred except for a surge of liquid in the experiment but not the calculation at about 10 s.

The calculated and measured broken loop cold leg fluid temperatures are compared in Figure 19. The temperatures both followed the local saturation temperature as the pressure decreased. Since the calculated pressure was below the measured pressure after 10 s the calculated temperature was also below the measured temperature. Figure 20 shows a comparison of lower plenum fluid temperatures. The rapid increase in the

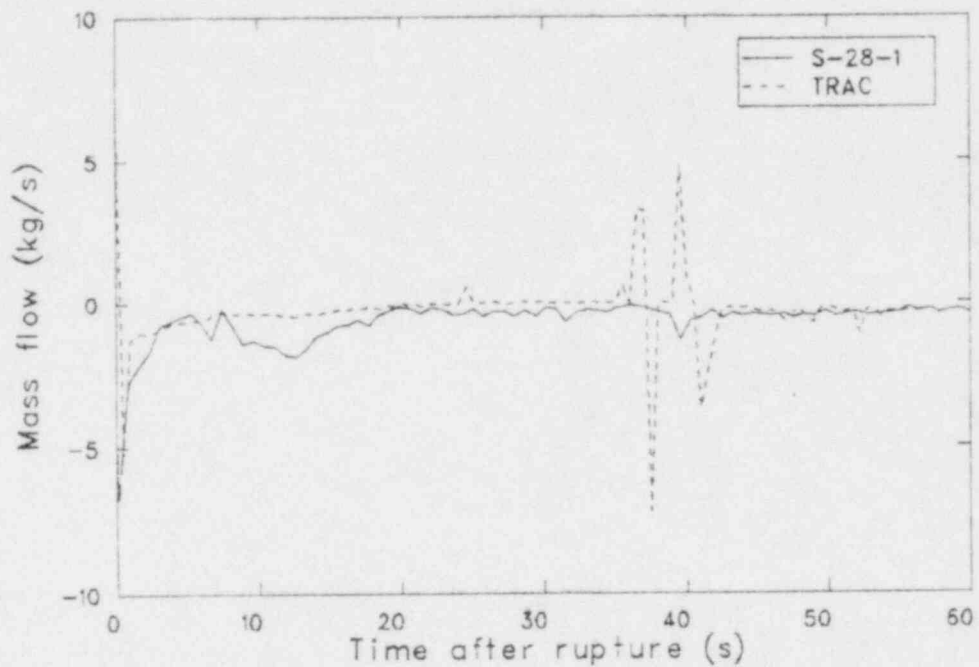


Figure 15. Comparison of the calculated and measured core inlet mass flow for Test S-28-1.

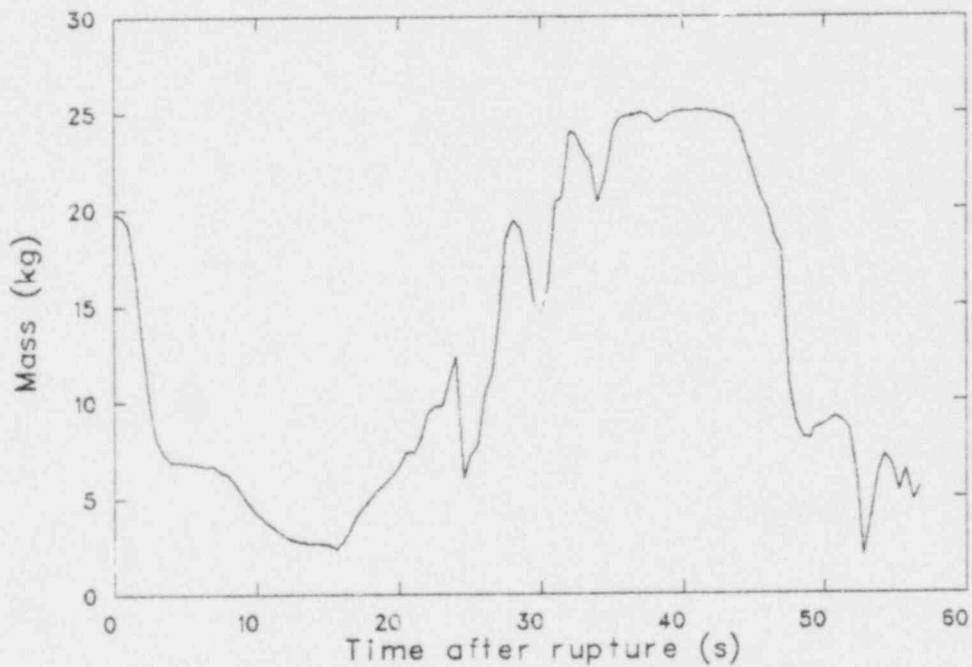


Figure 16. Calculated liquid mass in downcomer for Test S-28-1.

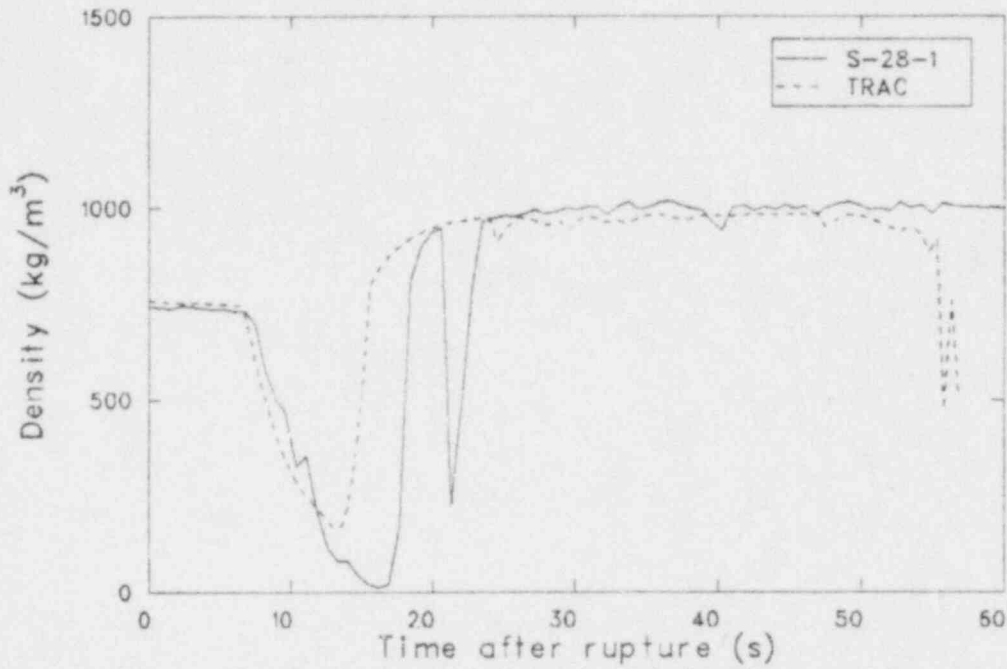


Figure 17. Comparison of the calculated and measured intact loop cold leg density for Test S-28-1.

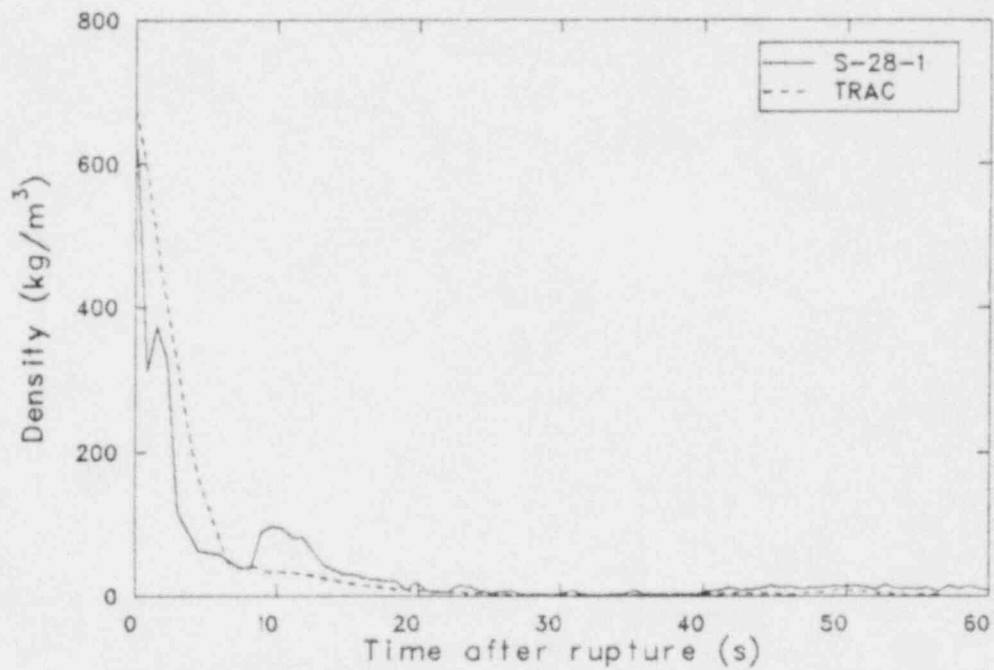


Figure 18. Comparison of the calculated and measured broken loop hot leg density for Test S-28-1.

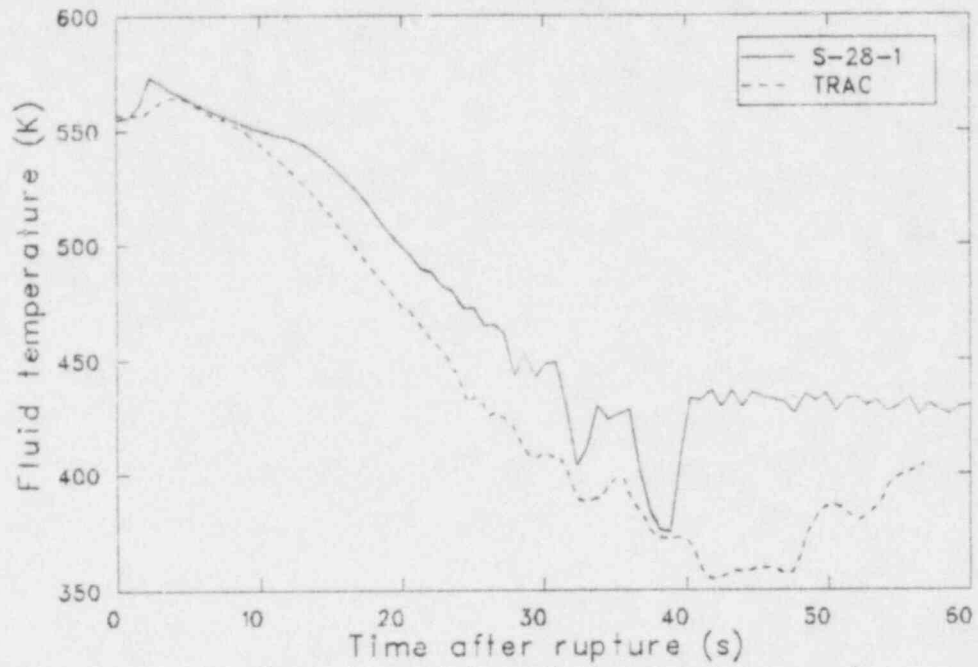


Figure 19. Comparison of the calculated and measured broken loop fluid temperature for Test S-28-1.

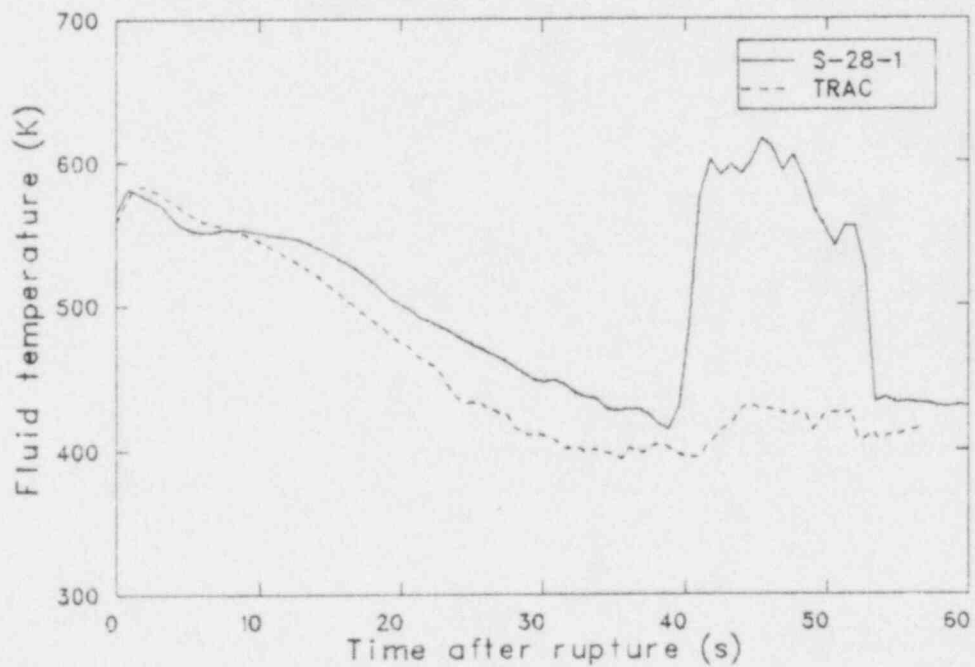


Figure 20. Comparison of the calculated and measured lower plenum fluid temperature for Test S-28-1.

measured temperature was caused by the reversal in core inlet flow at 39 s that was shown in Figure 15. Although the calculated flow reversal was larger, the calculated lower plenum temperature increase was not as large. This may be because the calculated flow reversal was of a shorter duration than for the measured flow.

One of the major features of TRAC-PD2 is the three-dimensional, two-fluid hydrodynamic methodology used in the reactor vessel component. The results of the calculation provide data on both the liquid and vapor velocities in axial, radial and azimuthal directions. Other fluid conditions such as pressure, temperature and void fraction were also calculated in each cell. Figure 21 shows an example of the calculated results in the vessel. This figure shows liquid velocities at 49.24 s in level 16 of the vessel, which was the level connected to the intact loop hot leg. At this time, the steam tube rupture fluid had already entered the vessel. The rupture fluid was shown flowing into the vessel through the intact hot leg. The void fraction in cell 4 was higher than in the intact loop hot leg and cell 8 to which it connected. The lower void fraction in cell 8 indicates that most of the liquid flowing in from the steam generator tube rupture flowed into cell 4 of the core. The volume of steam generator secondary liquid reaching the core was significantly less in the calculation than in the test. The preference for liquid to flow into the core sector adjacent to the intact hot leg in the calculation was not experimentally observed because sufficient liquid was available in the experiment to flood all core sectors equally.

4.1.2 Core Thermal Behavior

Comparisons between calculated and measured temperatures in the lower, middle, and upper core are shown in Figures 22 through 31.

Table 5 shows the maximum calculated and measured temperatures for selected core elevations and locations. In general the results shown in Table 5 indicate that the calculated maximum temperatures were slightly below the measured maximum temperatures. Table 6 summarizes the differences between the calculated and measured maximum temperatures.

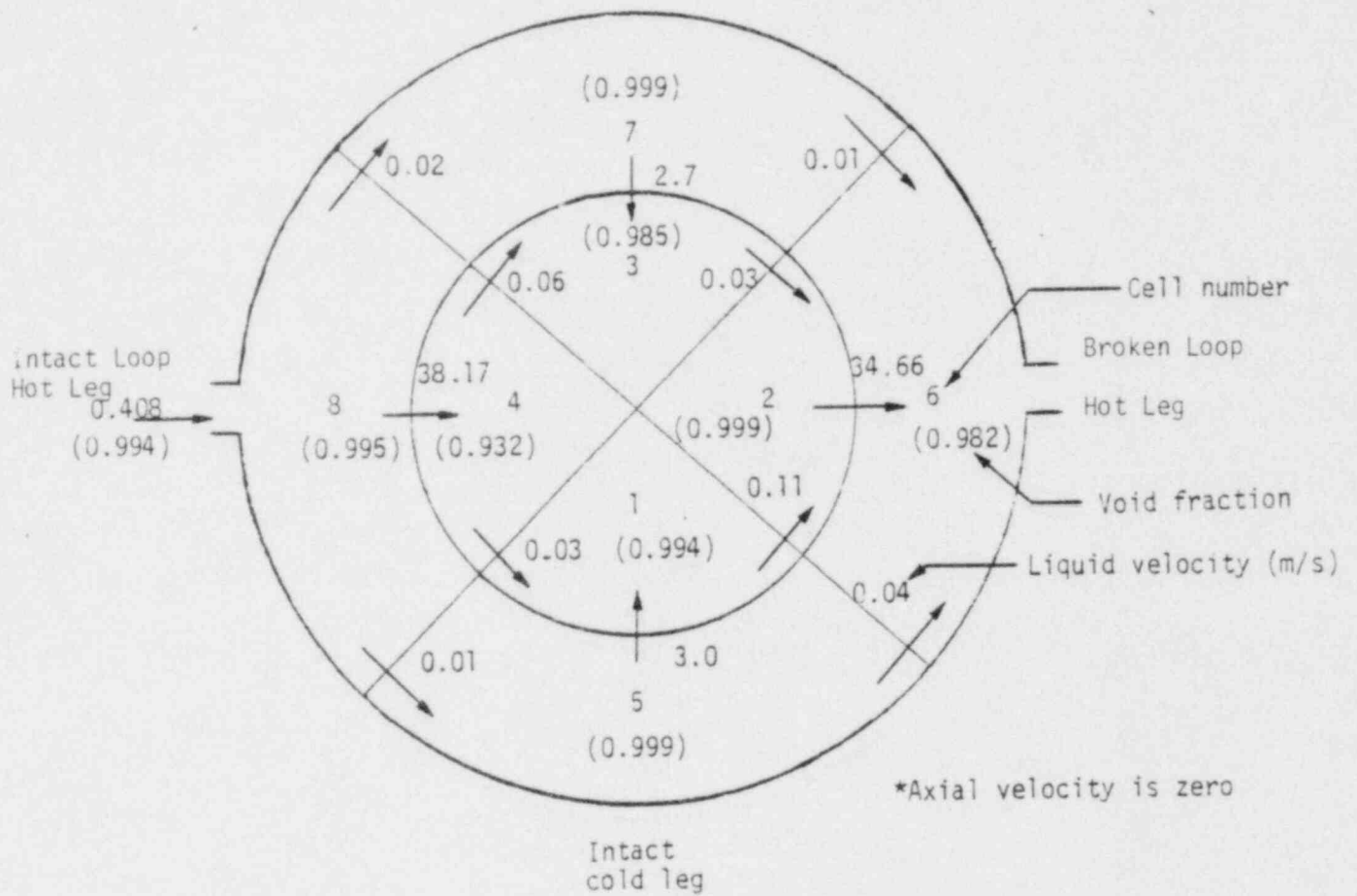


Figure 21. Liquid velocities and cell void fractions in vessel sixteen at 49.24 seconds obtained in the calculation for Test S-28-1.

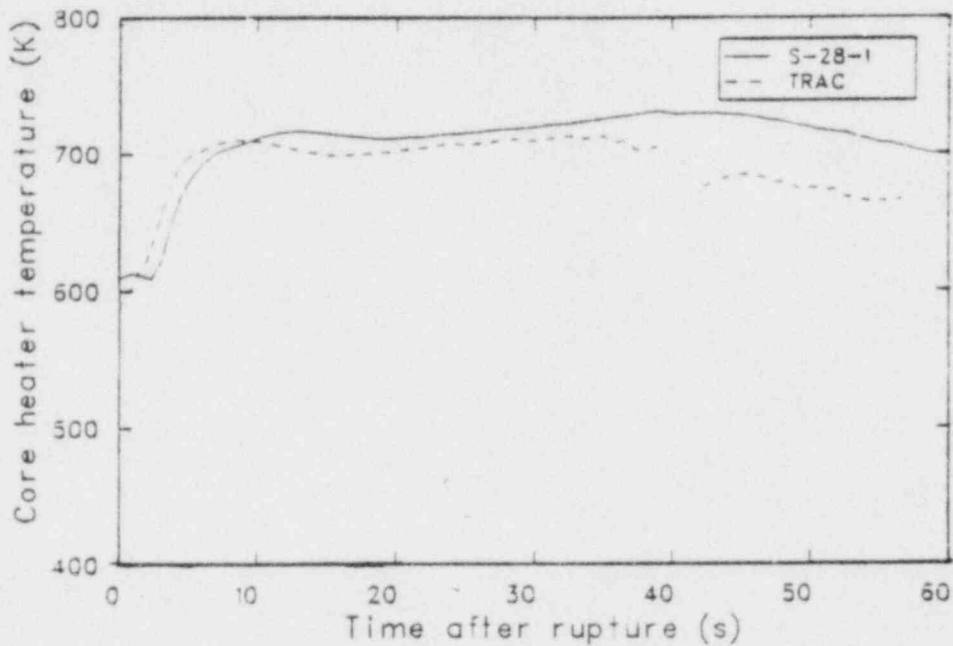


Figure 22. Comparison of the calculated and measured rod cladding temperature at first level of core region for Test S-28-1.

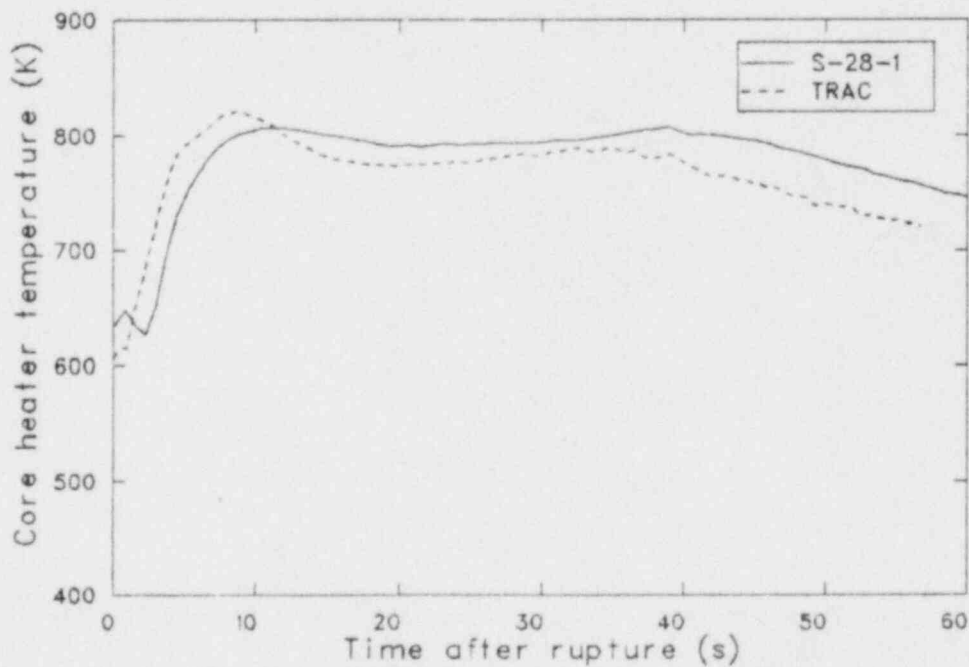


Figure 23. Comparison of the calculated and measured rod cladding temperature at second level of core region for Test S-28-1.

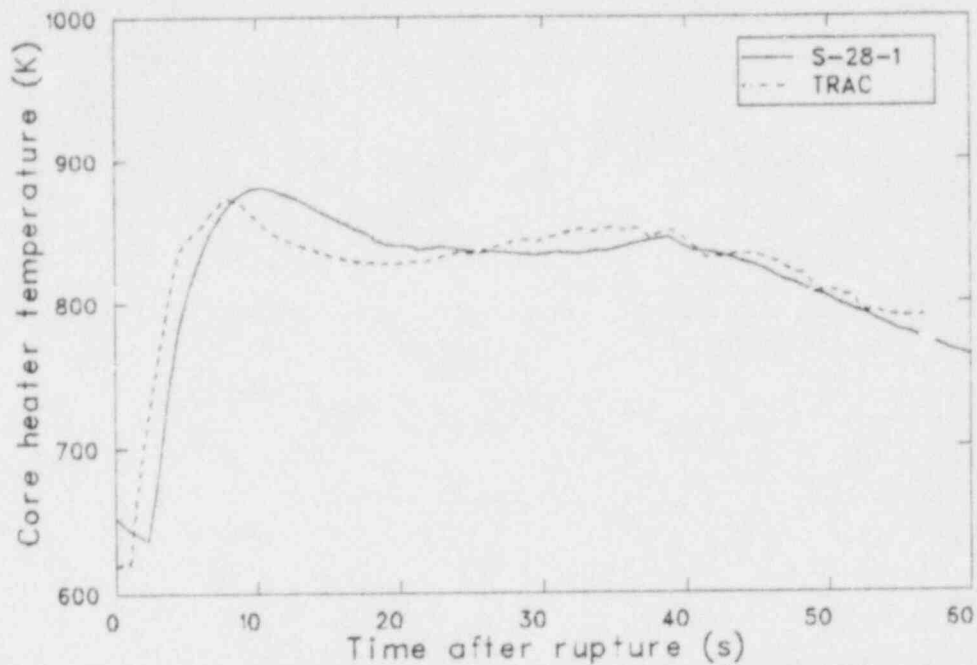


Figure 24. Comparison of the calculated and measured rod cladding temperature at third level of core region for Test S-28-1.

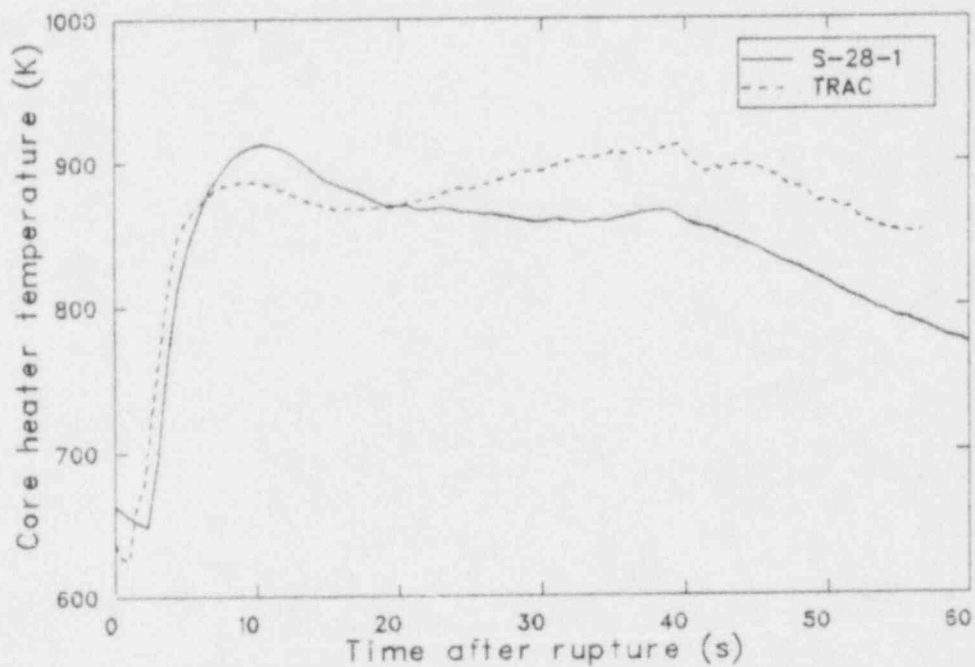


Figure 25. Comparison of the calculated and measured rod cladding temperature at fourth level of core region for Test S-28-1.

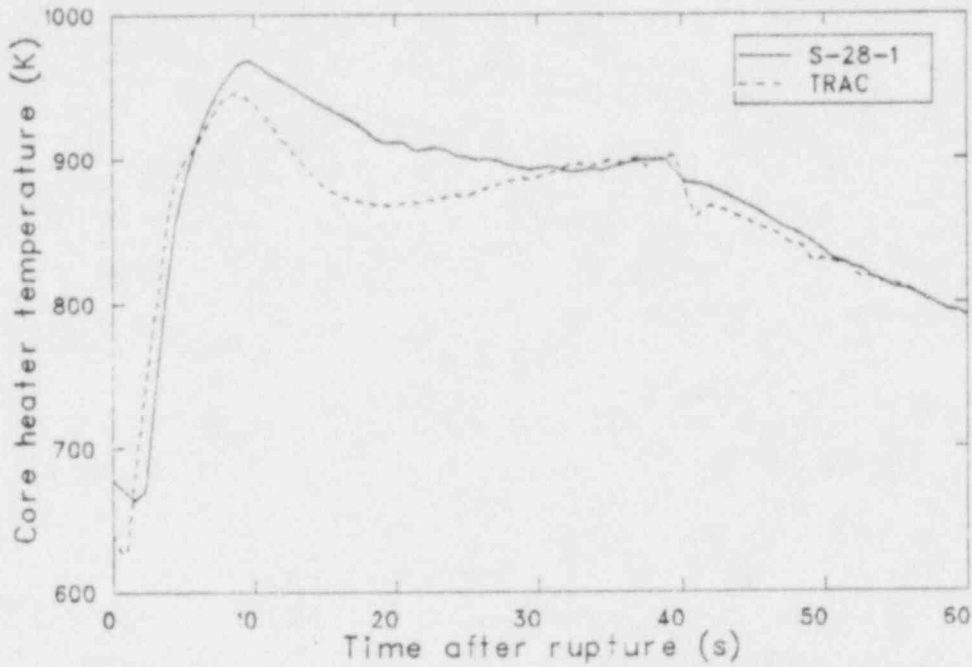


Figure 26. Comparison of the calculated and measured rod cladding temperature at fifth level of core region for Test S-28-1.

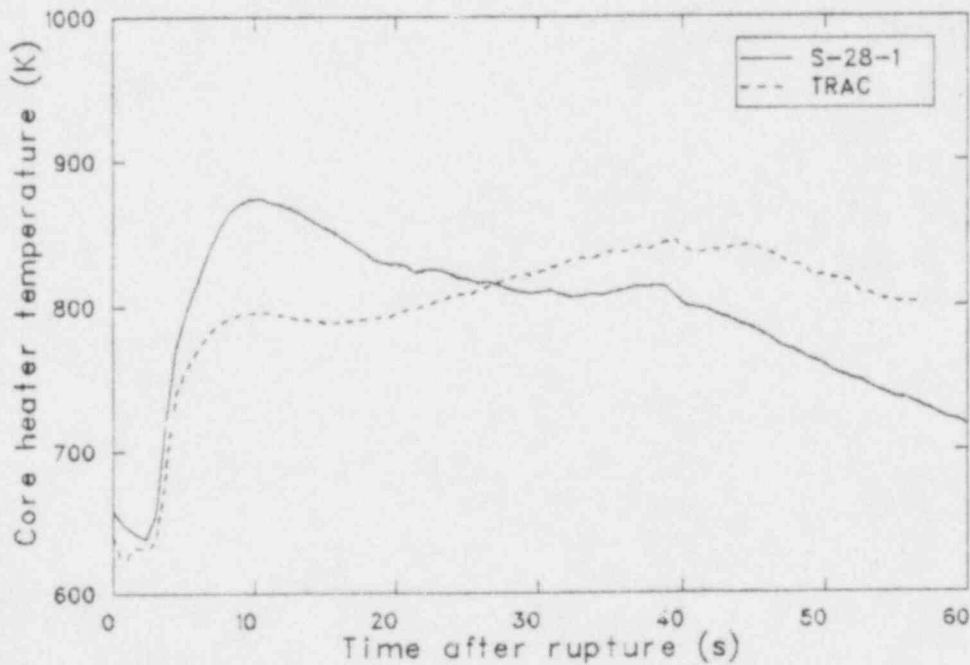


Figure 27. Comparison of the calculated and measured rod cladding temperature at sixth level of core region for Test S-28-1.

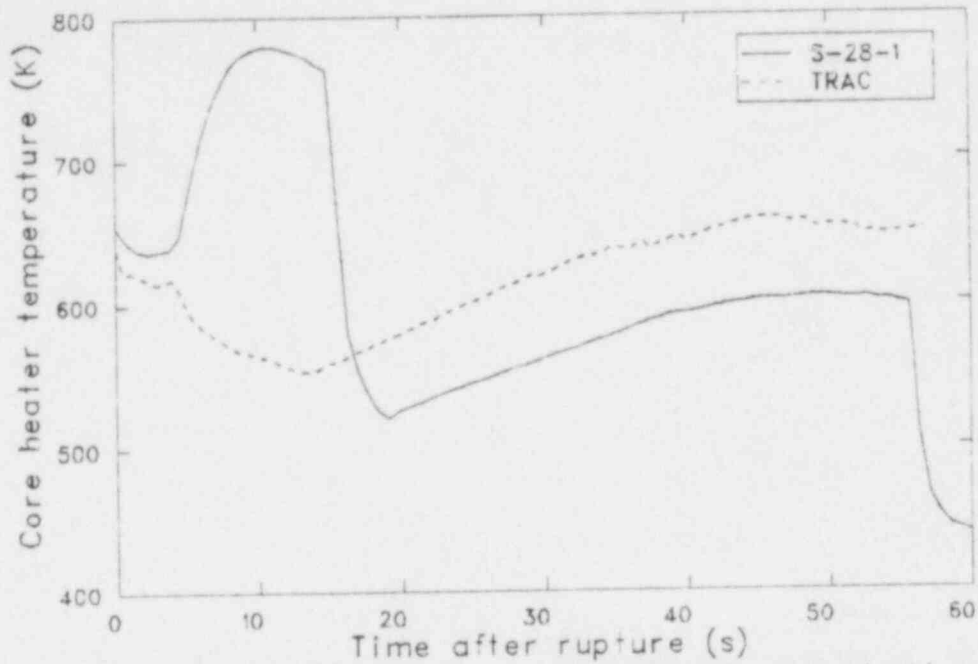


Figure 28. Comparison of the calculated and measured rod cladding temperature at seventh level of core region for Test S-28-1.

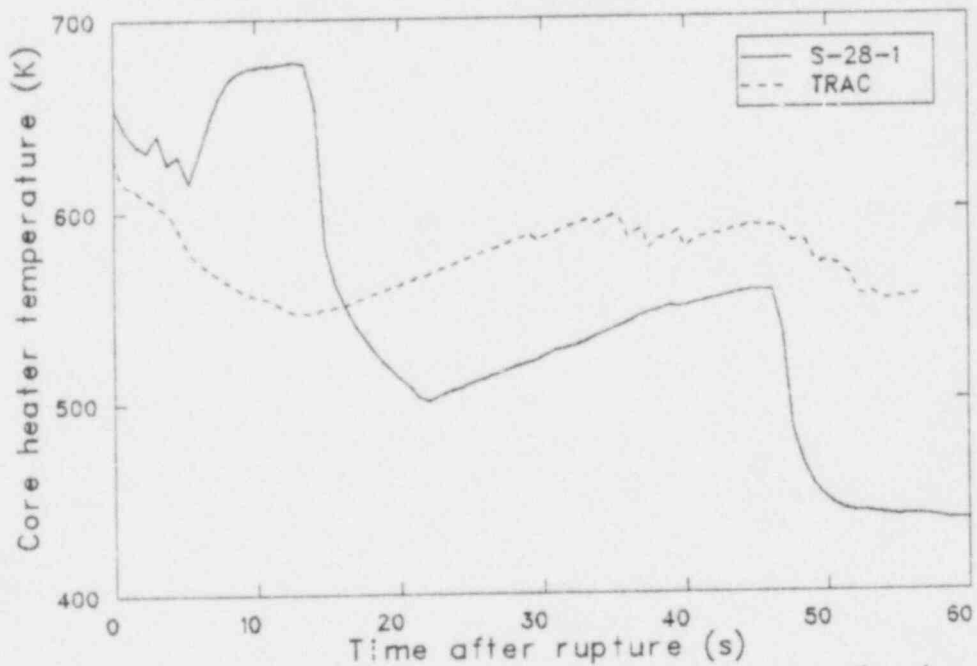


Figure 29. Comparison of the calculated and measured rod cladding temperature at eighth level of core region for Test S-28-1.

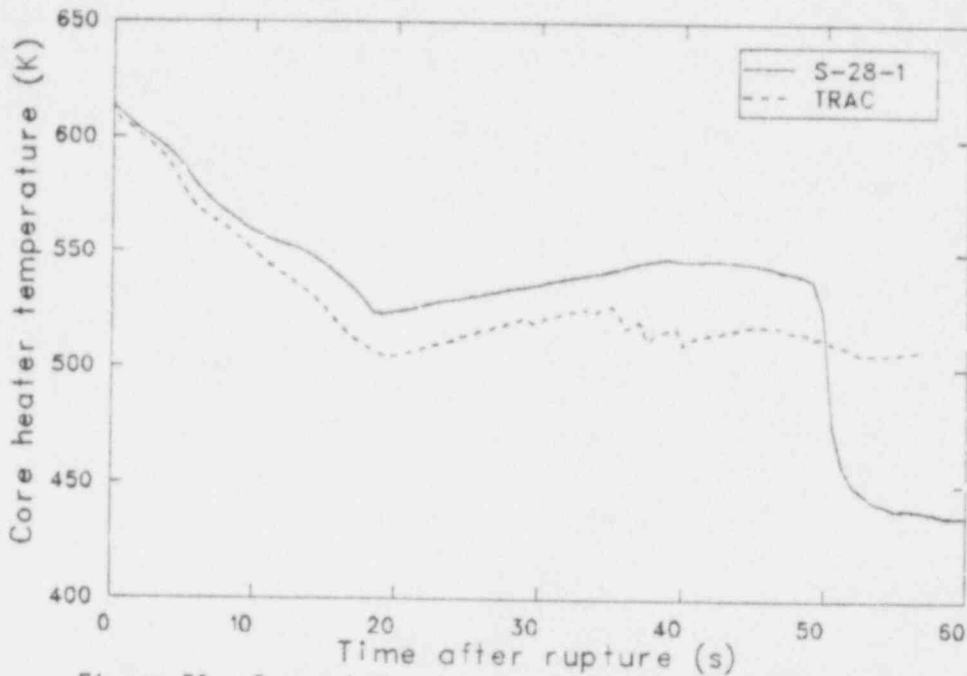


Figure 30. Comparison of the calculated and measured rod cladding temperature at ninth level of core region for Test S-28-1.

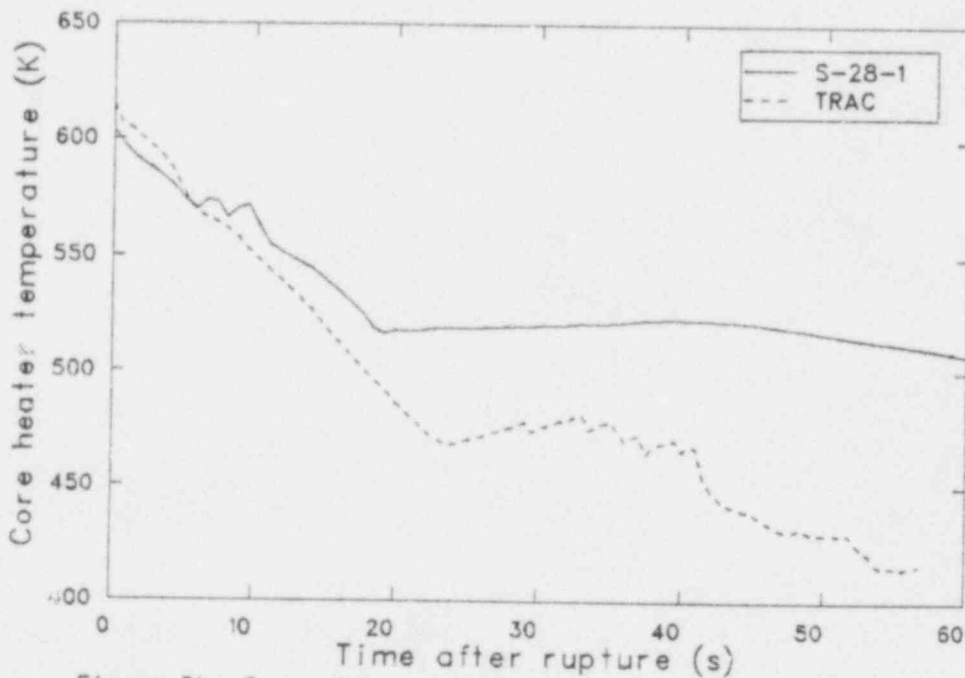


Figure 31. Comparison of the calculated and measured rod cladding temperature at tenth level of core region for Test S-28-1.

TABLE 5. MAXIMUM CORE TEMPERATURE AS A FUNCTION OF CORE LEVEL FOR TEST S-28-1

Core/Level	Hot Rod	Temperature (K)			
		Rod 1	Rod 2	Rod 3	Rod 4
1 c ^a	725.8	728.6	714.0	715.5	712.4
1 m ^b	--	--	--	710.0	--
2 c	820.4	820.7	802.0	805.1	799.5
2 m	800.0	860.0	--	760.0	925.0
3 c	893.4	896.4	873.2	878.8	870.2
3 m	900.0	960.0	900.0	960.0	--
4 c	935.9	942.4	911.8	919.7	910.5
4 m	950.0	1010.0	900.0	1020.0	920.0
5 c	945.1	956.3	897.7	917.0	911.8
5 m	980.0	1000.0	970.0	1040.0	1020.0
6 c	831.3	888.9	818.0	803.3	845.6
6 m	--	--	910.0	920.0	875.0
7 c	641.5	711.3	639.5	639.5	658.3
7 m	--	780.0	750.0	790.0	760.0
8 c	637.8	668.9	635.8	635.8	635.8
8 m	--	630.0	680.0	--	670.0
9 c	630.3	628.5	628.5	628.5	628.5
9 m	620.0	--	600.0	--	600.0
10 c	616.0	614.8	614.8	614.8	614.8
10 m	--	--	--	600.0	--
11 c	599.9	599.6	599.6	599.6	599.6

a. Calculated.

b. Measured.

TABLE 6. MAXIMUM CORE TEMPERATURE IN EACH CORE REGION FOR TEST S-28-1

	Temperature (K)				
	<u>Hot Rod</u>	<u>Rod 1</u>	<u>Rod 2</u>	<u>Rod 3</u>	<u>Rod 4</u>
Measured	980.0	1010.0	970.0	1020.0	1020.0
Calculated	945.1	956.3	911.8	919.7	911.8
% Error	3.0	5.3	6.0	11.0	10.0

Table 7 lists the occurrence of critical heat flux (CHF) in the experiment and calculation. In the experiment CHF occurred in the lower and middle core (up to level 8). Above level 8 the heater rods remained in nucleate boiling. In the calculation CHF only occurred up to the sixth level. In general, the calculated and measured temperatures were in good agreement in levels 1 through 5, 9, and 10. In levels 6 through 8 differences in CHF occurred and temperature comparisons were poor. Reference 6 discussed the relationship between the agreement of the calculation of CHF and the overall temperature comparisons. For example, Figure 24 shows a comparison of rod temperatures at the third core level where CHF occurred in both the experiment and calculation. Figure 30 shows the same comparison at the ninth core level where CHF did not occur in either the experiment or calculation. These figures show relatively good agreement in the temperature response. Figure 28 shows a comparison at the seventh level where the CHF was measured but was not calculated. The comparison of the temperature response at this level was poor.

Although a flat radial power profile was used in the TRAC-PD2 model, identical temperature responses were not calculated for the four modeled rods. Figure 32 shows the differences in the calculated midcore cladding temperatures between the four rods. The responses for the four rods were identical for the first 6 s of the transient when all the rods were in nucleate boiling. Differences occurred after 6 s when the rods experienced transition and film boiling. After 40 s, when the steam generator tubes were ruptured, the rod 3 behavior deviates significantly from the others. Differences of this nature exist at other levels as well and have not been explained. The previously identified preference for the injected liquid to flow into the core sector adjacent to the intact hot leg was not apparent at the lower vessel locations. The asymmetry may be a result of the input, which was identified after the calculation was performed. At the recent TRAC workshop it was noted that core azimuth sections must be defined in radians to fourteen significant figures to avoid azimuthal calculational irregularities. The input for this calculation was to four significant figures, and this may be a partial cause for some of the differences shown in Figure 32.

TABLE 7. COMPARISON OF CALCULATED AND MEASURED CHF FOR TEST S-28-1

Core/Level	Hot Rod	Rod 1	Rod 2	Rod 3	Rod 4
1 c ^a	Y ^c	Y	Y	Y	Y
1 m ^b	Y	Y	Y	Y	Y
2 c	Y	Y	Y	Y	Y
2 m	Y	Y	Y	Y	Y
3 c	Y	Y	Y	Y	Y
3 m	Y	Y	Y	Y	Y
4 c	Y	Y	Y	Y	Y
4 m	Y	Y	Y	Y	Y
5 c	Y	Y	Y	Y	Y
5 m	Y	Y	Y	Y	Y
6 c	Y	Y	Y	Y	Y
6 m	-- ^d	Y	Y	Y	Y
7 c	N ^e	N	N	N	N
7 m	--	Y	Y	Y	Y
8 c	N	N	N	N	N
8 m	--	Y	Y	--	Y
9 c	N	N	N	N	N
9 m	N	--	N	--	N
10 c	N	N	N	N	N
10 m	N	--	N	N	--
11 c	N	N	N	N	N

a. Calculated.

b. Measured.

c. CHF occurrence.

d. No data available.

e. No CHF.

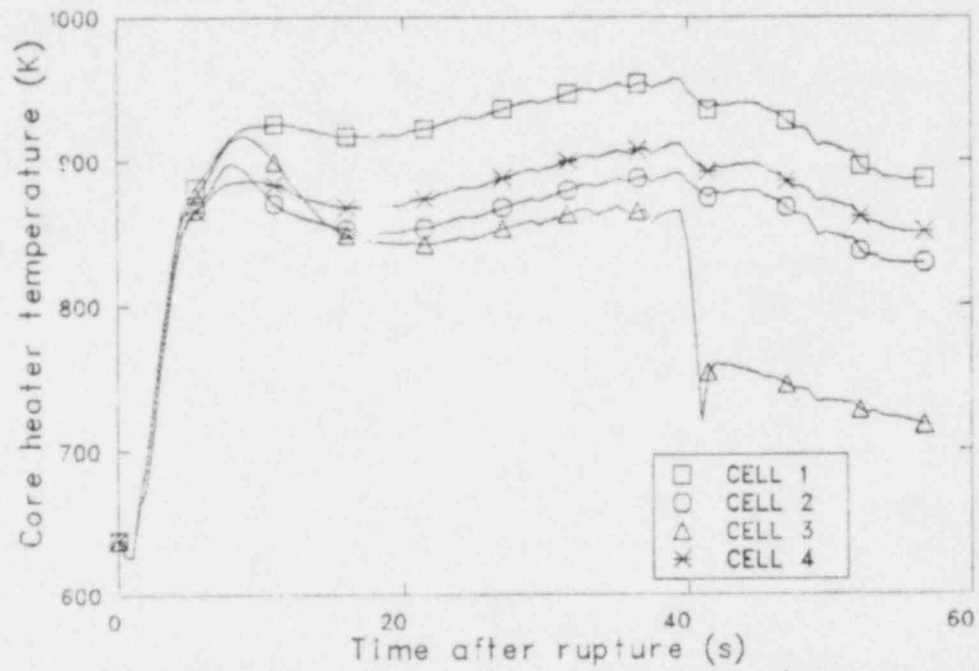


Figure 32. Calculation cladding temperatures of average core heater rods at middle core elevation for Test S-28-1.

In the experiment, quench of the top core levels occurred following the steam generator tube ruptures at 40 s. The quench was caused by secondary fluid entering the ruptured steam generator tubes, flowing through the intact hot leg and into the top of the core. Table 8 summarizes the downward progression of this top down quench which is also shown in Figs 28 through 31. For Test S-28-1, the sixty ruptured steam generator tubes provided sufficient flow of water to the upper plenum that no radial or azimuthal preferential core quenching occurred in the test. Thus, a strictly top down quench was measured in the experiment. In the calculation a top down quench was also calculated as shown in Table 9. The calculated top down quench began later and proceeded slower than in the experiment. It appears this difference was a result of an improper calculation of the flashing rate when the hot steam generator fluid was injected into the intact hot leg. Too high a flashing rate was calculated causing too much of the injected liquid to be flashed and leaving little liquid for quenching the core. The calculated core temperature response in the middle and lower core regions agreed well with the experiment as shown in Figures 22 through 26.

4.2 Test S-28-10 Rupture of Twelve Steam Generator Tubes

In this section, the TRAC-PD2 calculations of Test S-28-10 are compared with data. The presentations follow the same format as for Test S-28-1. Results of this calculation are stored on Tape A41931 and the graphic files are stored on Tapes A32452/A32284. The calculation was terminated after 120 s of the transient because the calculation was running very slowly.

4.2.1 System Hydraulic Response

Figure 33 shows a comparison of experimental and calculated primary system pressures and Figure 34 shows a comparison of broken loop cold leg mass flow rates. The calculated system pressure was lower than the measured pressure from about 2 s to 24 s. The calculated broken loop mass flow rate was lower than the measured flow for the initial 2 s of the

TABLE 8. QUENCH TIME AS A FUNCTION OF CORE ELEVATION AT CORE HEATER ROD REGION FOUR FOR TEST S-28-1

Core Elevation (m)	Quench Time (s)
1.346	43
0.66	68
0.508	80

TABLE 9. CALCULATED QUENCH TIME AS A FUNCTION OF CORE ELEVATION AT CORE HEATER ROD FOUR FOR TEST S-28-1

Core Elevation (m)	Quench Time (s)
1.676	47
1.422	50
1.218	52
1.042	>60

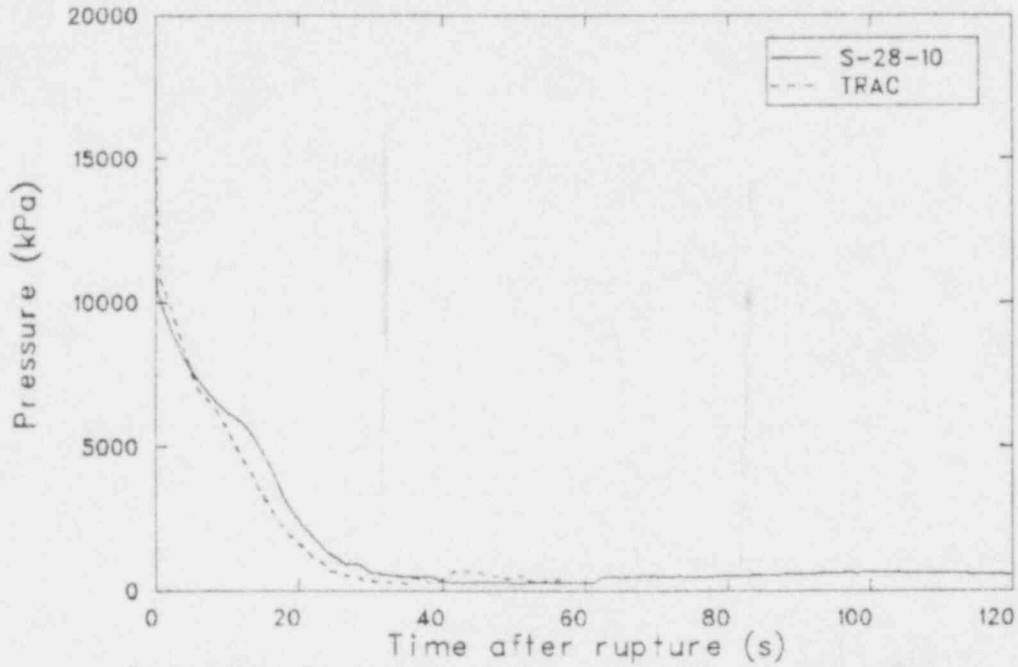


Figure 33. Comparison of the calculated and measured system pressure response for Test S-28-10.

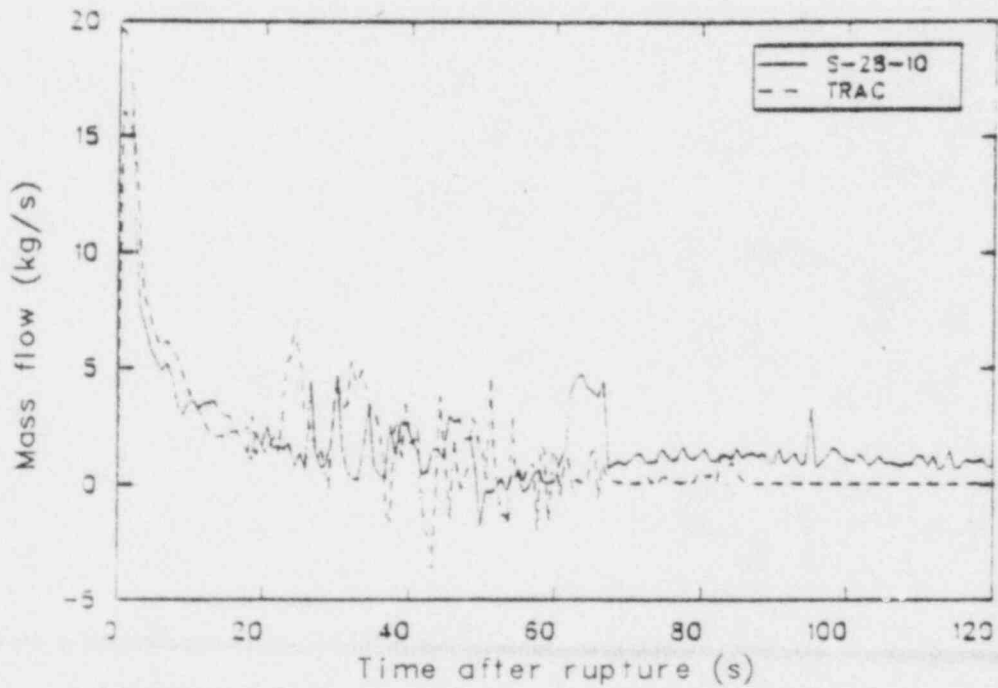


Figure 34. Comparison of the calculated and measured broken loop cold leg mass flow for Test S-28-10.

transient and higher than the measured from 2 s to 14 s. The difference between the calculated and measured broken loop mass flow rate contributed to the difference in the pressure response.

The intact and broken loop accumulator injection rates are shown in Figures 35 and 36, respectively. The results were similar to those obtained for Test S-28-1. In the intact loop, the measured accumulator liquid depletion time was 64 s and the calculated time was 35 s. This calculated depletion time was shorter than the 48 s calculated for Test S-28-1 because, for Test S-28-10, the accumulator injection line flow resistance was decreased to correct an error. However, this change resulted in an even higher accumulator discharge rate and a worse comparison of liquid depletion times.

The intact loop hot leg mass flow comparison is shown in Figure 37. When these results are compared with the results for Test S-28-1, in Figure 11 it is observed the calculation for Test S-28-10 more closely agreed with the data during the period from 10 to 40 s. Since the only difference in the calculations during this period was the change in accumulator injection line resistance, the improvement in the mass flow comparison is attributed to it. In the intact cold leg, the mass flow comparison (Figure 38) is similar to that obtained for S-28-1 as shown in Figure 12.

Also because of the decrease in injection line resistance, the calculated refilling of the intact loop cold leg (Figure 39) occurred earlier than for Test S-28-1.

A comparison of the core inlet mass flows, shown in Figure 40, indicates good agreement up to 30 s. Between 30 s and 55 s the calculation oscillated more than the test. This difference was caused by the initiation of reflooding at 35 s in the calculation, whereas, reflood occurred at 55 s in the test. The earlier calculated reflood was caused by an early intact loop accumulator initiation time and higher injected flow

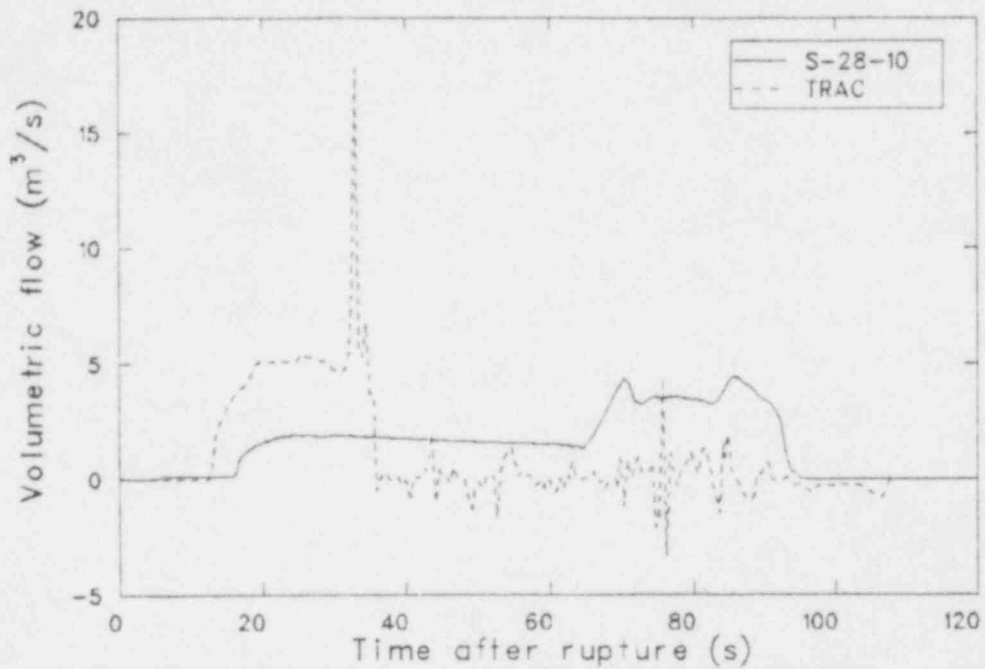


Figure 35. Comparison of the calculated and measured intact loop accumulator discharge volumetric flow for Test S-28-10.

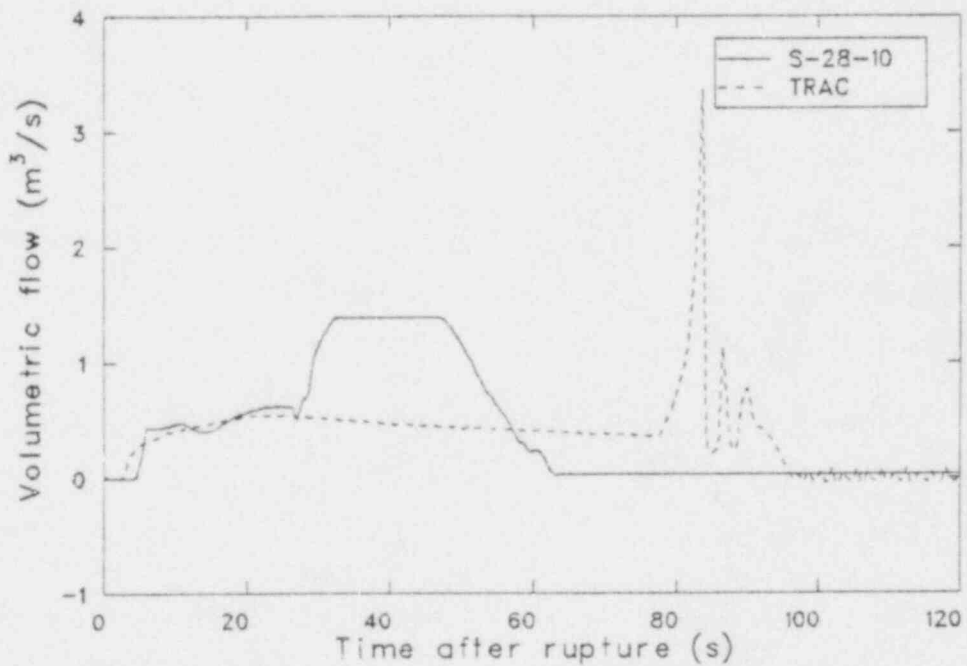


Figure 36. Comparison of the calculated and measured broken loop accumulator discharge volumetric flow for Test S-28-10.

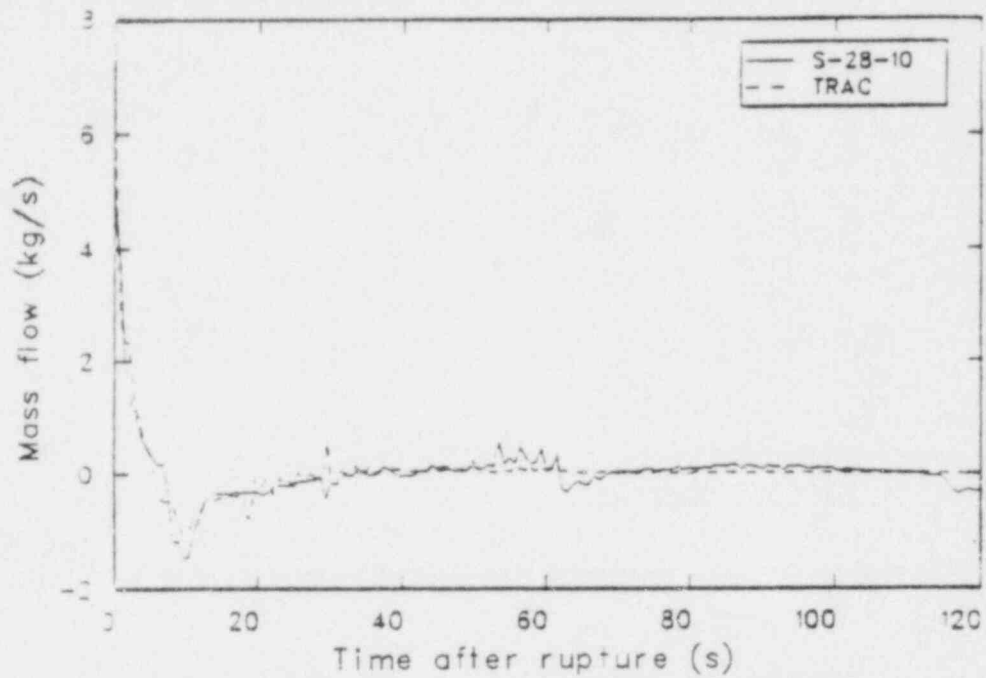


Figure 37. Comparison of the calculated and measured intact loop hot leg mass flow for Test S-28-10.

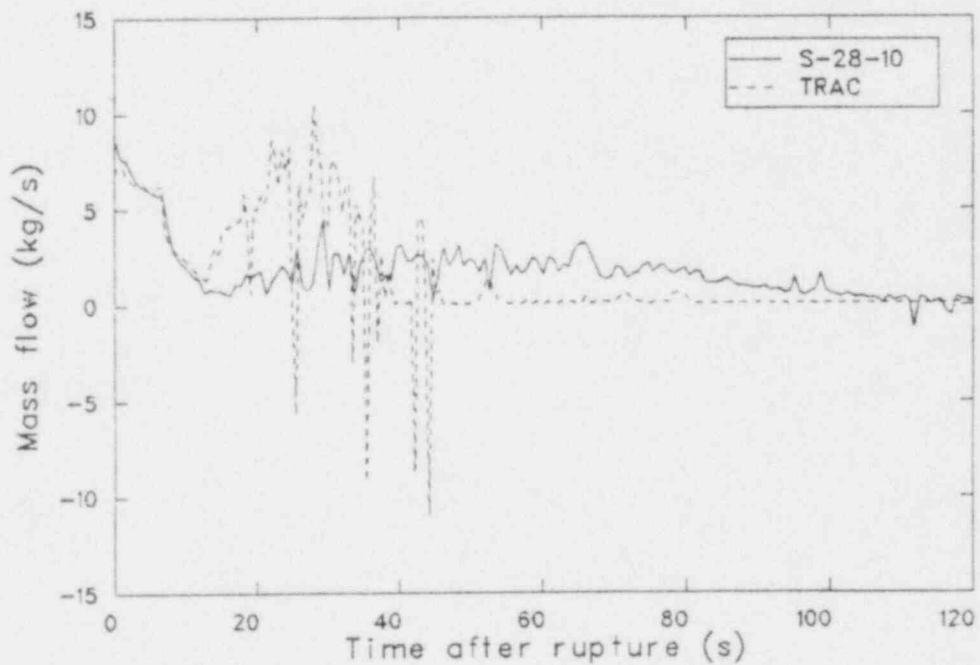


Figure 38. Comparison of the calculated and measured intact loop cold leg mass flow for Test S-28-10.

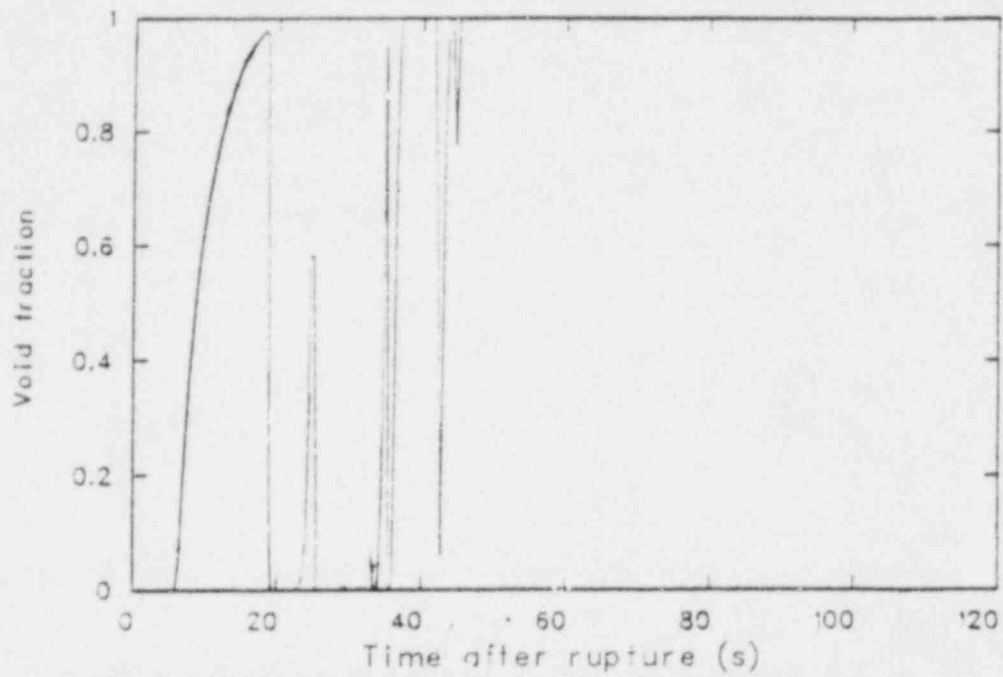


Figure 39. Calculated void fraction in intact loop cold leg upstream of ECC injection location for Test S-28-10.

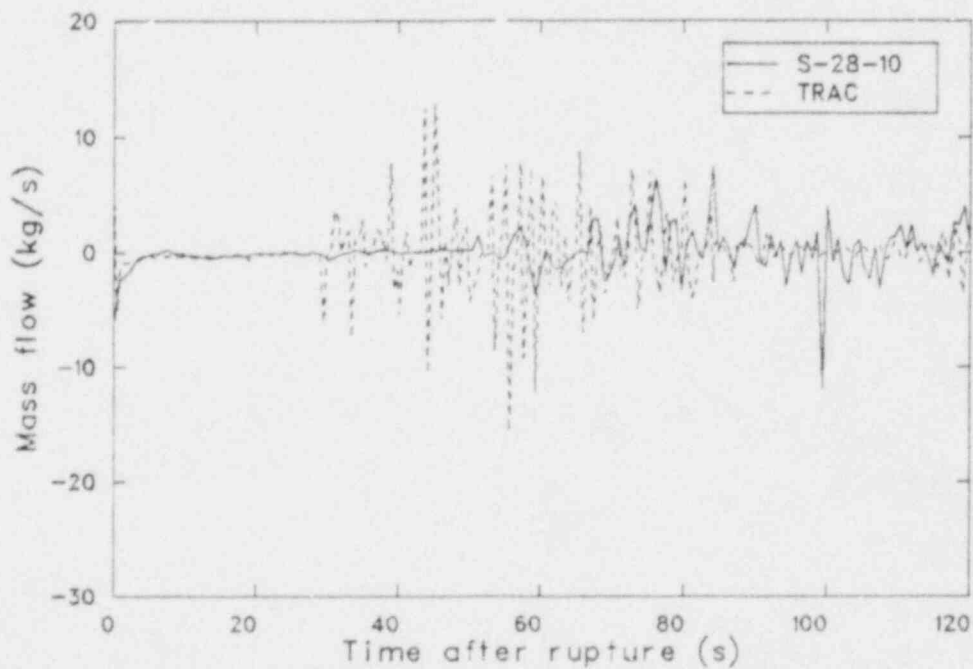


Figure 40. Comparison of the calculated and measured core inlet mass flow for Test S-28-10.

rate. The earlier initiation of reflooding in the calculation than in the experiment was also indicated by the core inlet density comparison shown in Figure 41.

Figure 42 shows a comparison of intact loop cold leg densities. The differences between 16 and 22 s were the result of the earlier accumulator injection. Between 35 and 70 s the differences were caused by the earlier termination of accumulator injection in the calculation than in the experiment.

Figure 43 shows a comparison of lower plenum fluid temperatures. Since the primary system depressurized faster in the calculation than in the test and because the primary fluid temperature followed the saturation temperature, the calculated fluid temperature was generally below the measured temperature.

4.2.2 Core Thermal Behavior

Comparisons between calculated and measured core temperatures are shown in Figures 44 through 51. Unlike Test S-28-1 where 60 tubes were simulated to be ruptured, the injection rate based on 12 ruptured tubes was insufficient to cause a top down quench in either the experiment or calculation. The core reflood began at 35 s in the calculation and 55 s in the test.

In the bottom of the core a significant difference occurred in the temperature comparison during the first 3 s of the transient. Figure 44 shows that the calculated temperature rapidly increased during this period, whereas, the measured temperature was nearly constant. This result indicates that CHF was calculated at the initiation of the transient, whereas, a delayed CHF was measured. The differences between the calculated and measured CHF was not as large at elevations from the second to sixth core levels as shown in Figures 45 through 49.

A summary of measured and calculated core quench times is shown in Table 10. None of the elevations above Level 4 were calculated to have

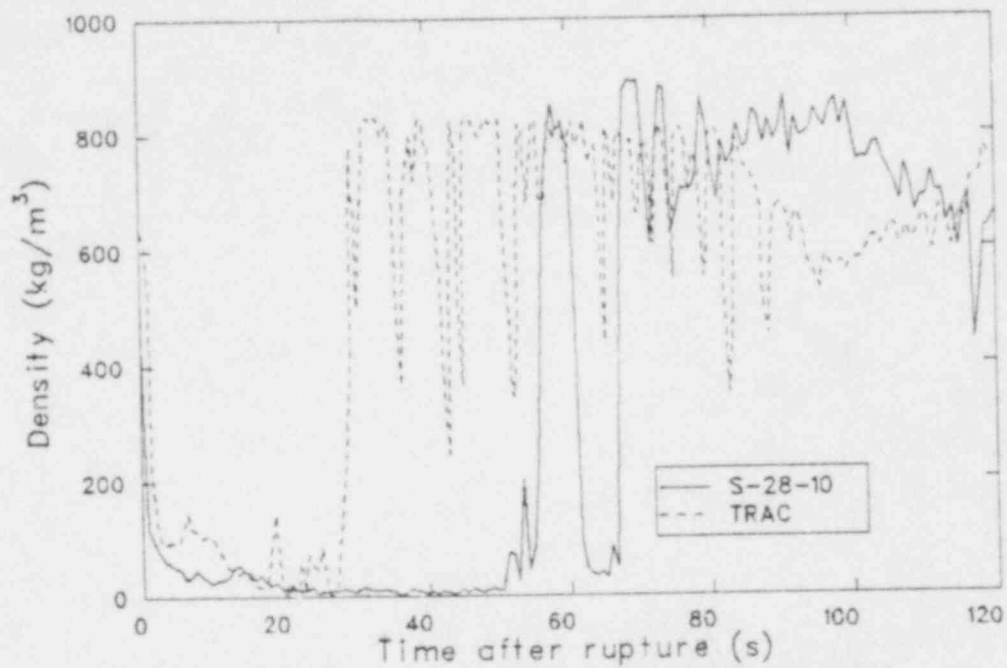


Figure 41. Comparison of the calculated and measured core inlet density for Test S-28-10.

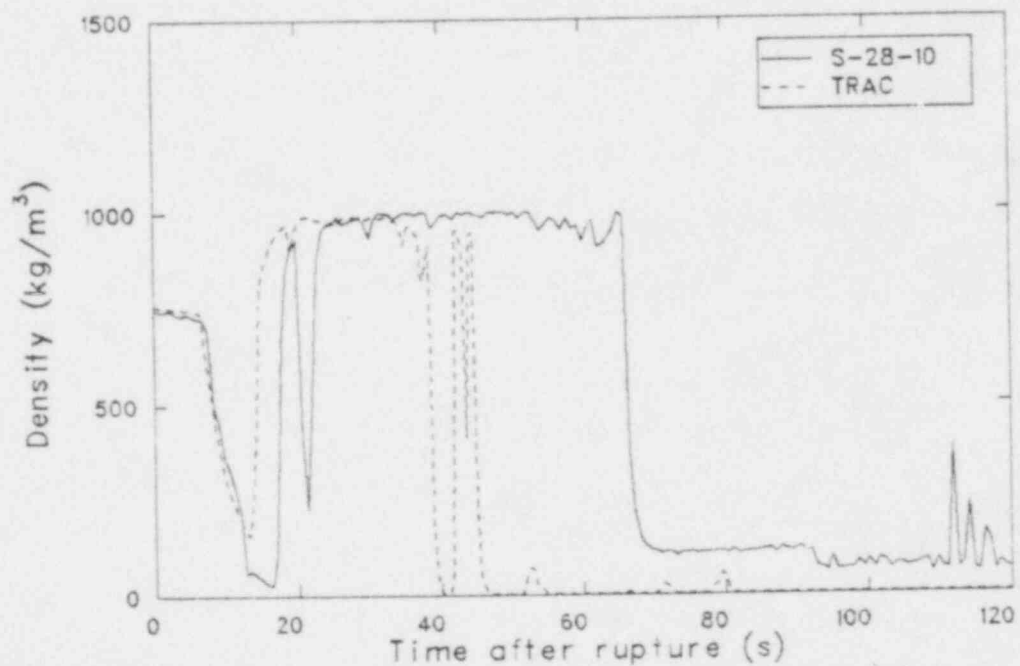


Figure 42. Comparison of the calculated and measured intact loop cold leg density for Test S-28-10.

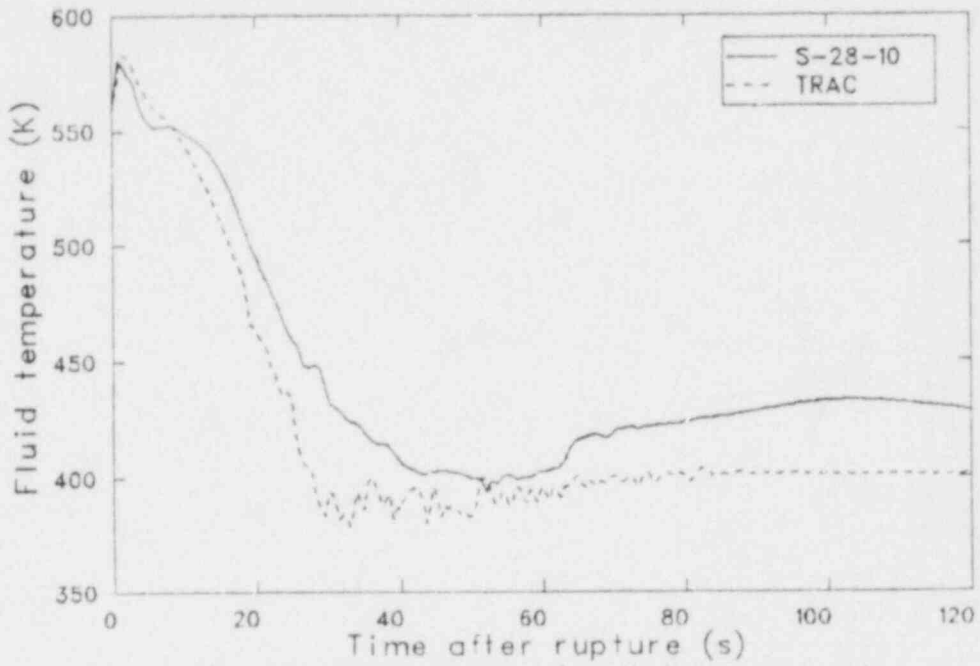


Figure 43. Comparison of the calculated and measured lower plenum fluid temperature for Test S-28-10.

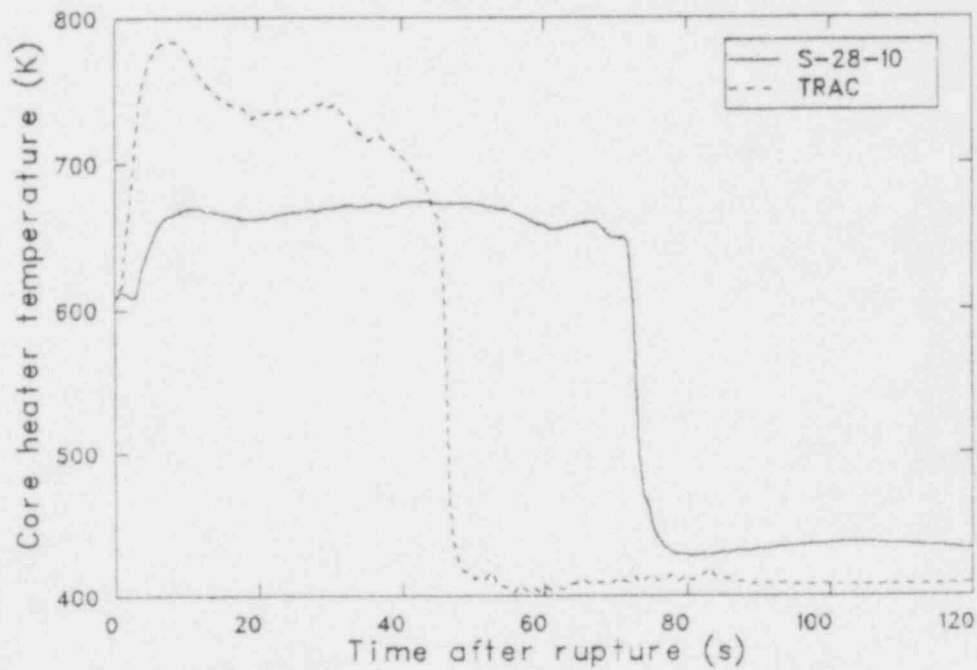


Figure 44. Comparison of the calculated and measured rod cladding temperature at first level of core region for Test S-28-10.

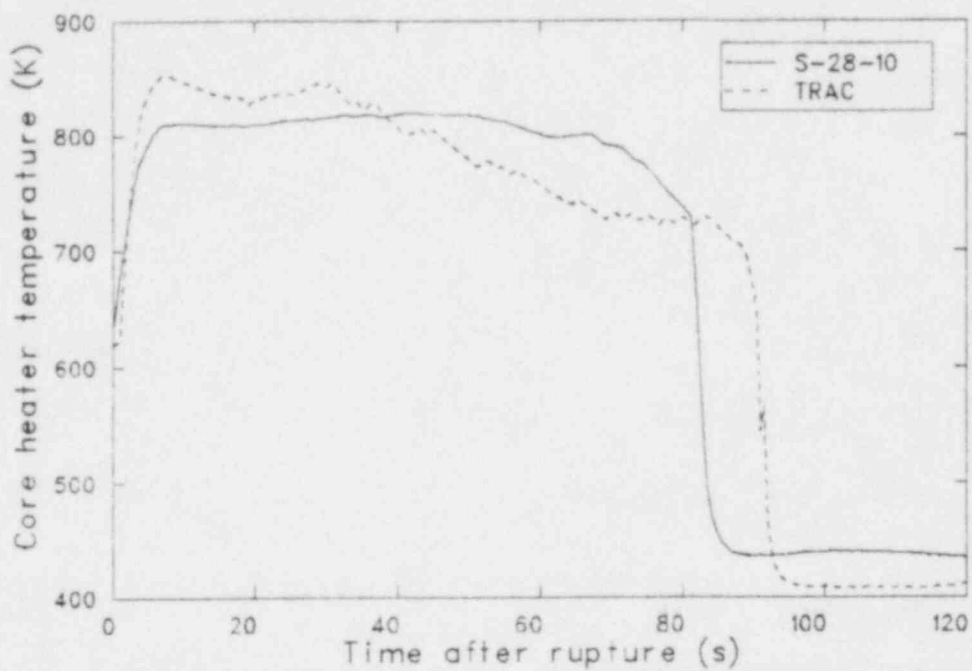


Figure 45. Comparison of the calculated and measured rod cladding temperature at second level of core region for Test S-28-10.

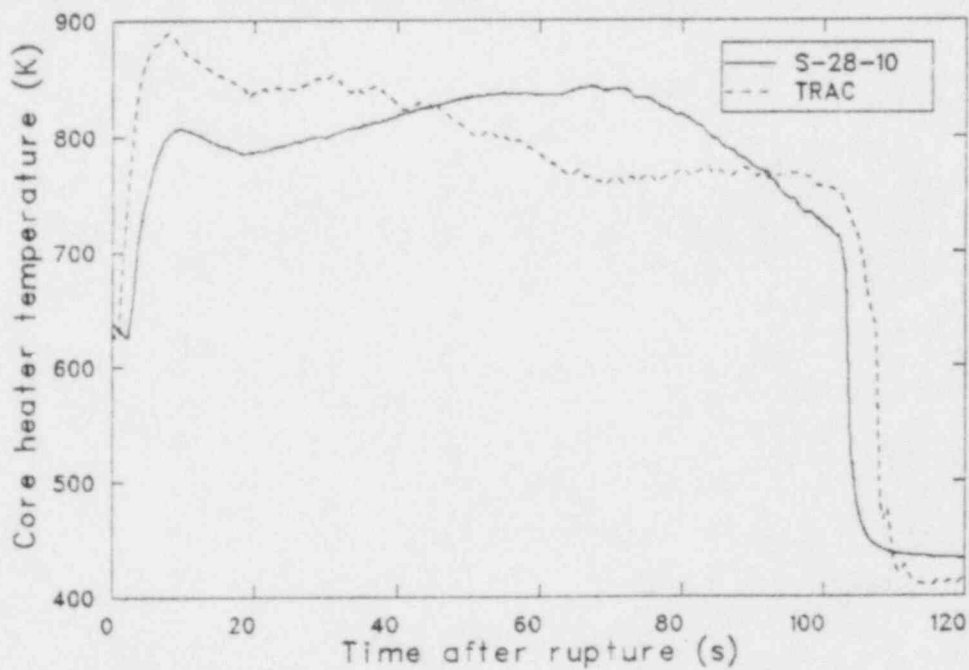


Figure 46. Comparison of the calculated and measured rod cladding temperature at third level of core region for Test S-28-10.

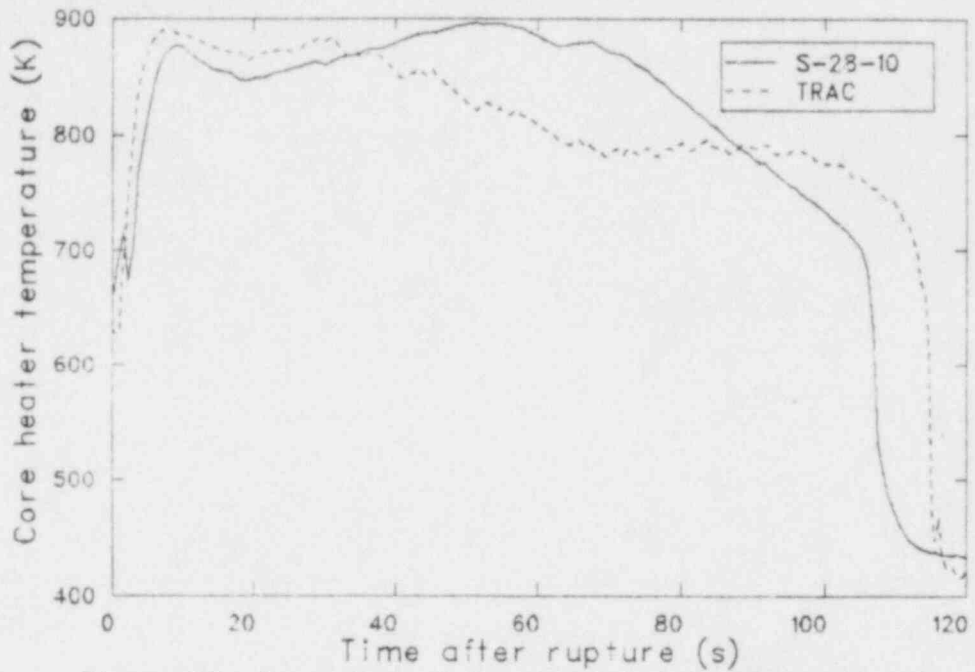


Figure 47. Comparison of the calculated and measured rod cladding temperature at fourth level of core region for Test S-28-10.

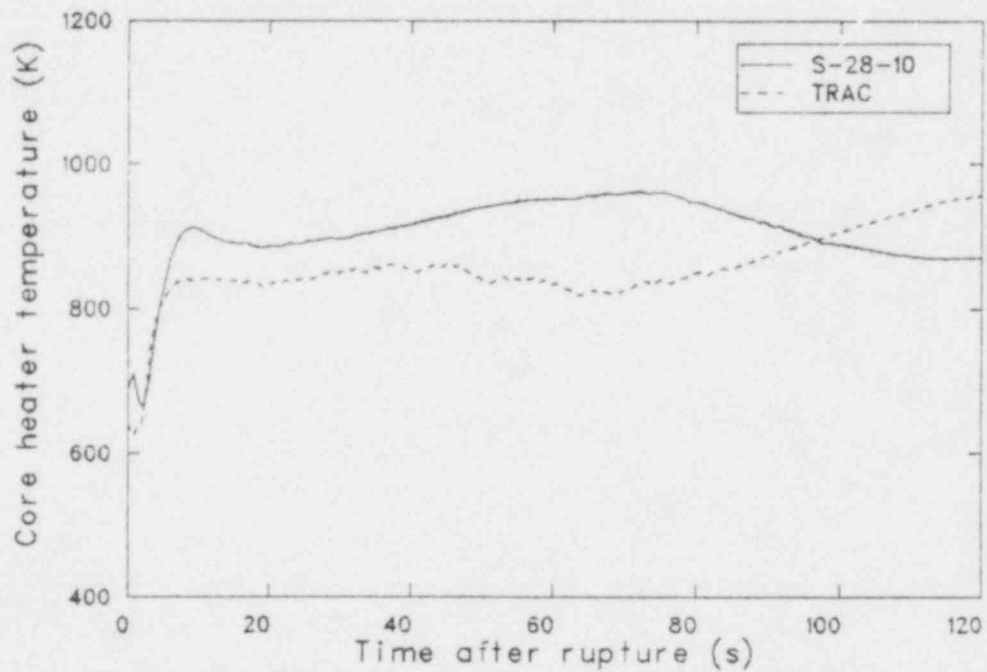


Figure 48. Comparison of the calculated and measured rod cladding temperature at fifth level of core region for Test S-28-10.

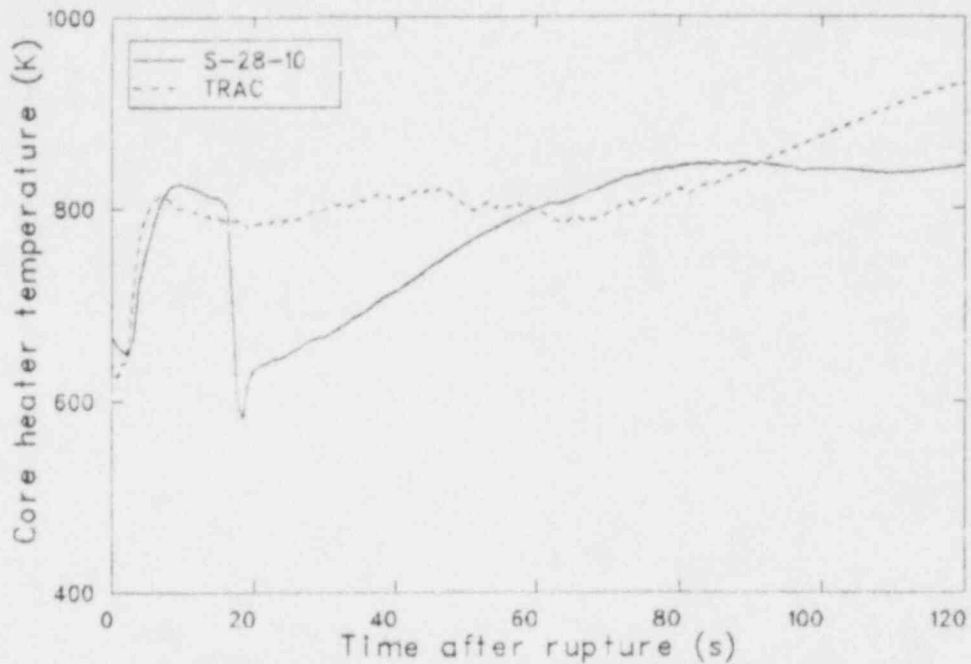


Figure 49. Comparison of the calculated and measured rod cladding temperature at sixth level of the core region for Test S-28-10.

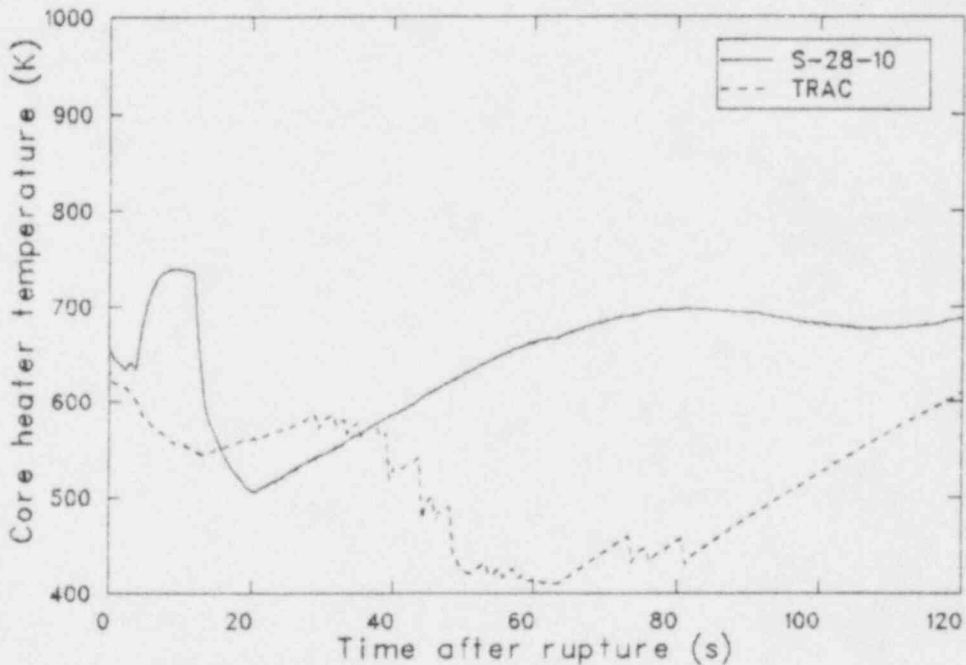


Figure 50. Comparison of the calculated and measured rod cladding temperature at seventh level of core region for Test S-28-10.

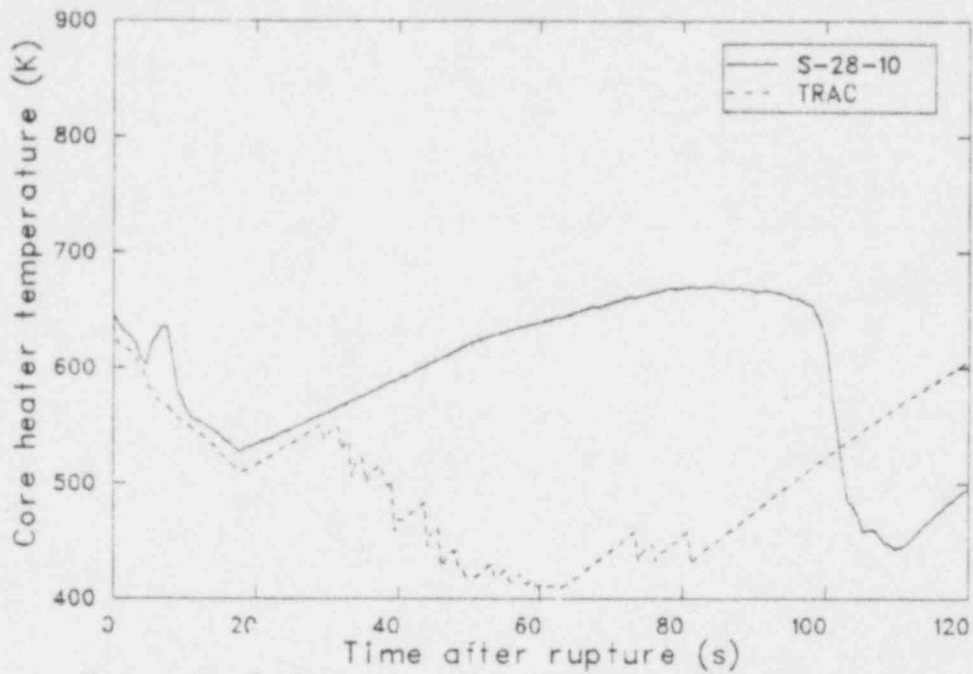


Figure 51. Comparison of the calculated and measured rod cladding temperature at eighth level of core region for Test S-28-10.

TABLE 10. QUENCH TIME AS FUNCTION OF CORE ELEVATION FOR TEST S-28-10

Core/Level	Time (s)				
	Rod 1	Rod 2	Rod 3	Rod 4	Hot Rod
1 c ^a	37.5	35.0	35.0	35.0	35.0
m ^b	-- ^c	--	70.0		
2 c	60.0	54.0	50.0	50.0	50.0
m	80.0	--	80.0	90.0	80.0
3 c	90.0	80.0	67.0	80.0	78.0
m	100.0	100.0	100.0	--	100.0
4 c	115.0	107.0	98.0	107.0	105.0
m	110.0	110.0	110.0	100.0	110.0

a. Calculated.

b. Measured.

c. No data available.

quenched by 120 s when the calculation was terminated. The early calculated quench times, caused by early accumulator injection and excessive injection rate, are evident at most rod elevations.

Table 11 provides a summary of peak cladding temperatures in the lower half of the core. The comparisons were generally good. Peak cladding temperatures were overpredicted for some rods and underpredicted for other rods at each elevation. The bottom quench process had not yet reached levels above Level 4 by the termination of the calculation at 120 s.

A summary of critical heat flux (CHF) is shown in Table 12. In the experiment, CHF occurred in the lower and middle core up to Level 8. Levels 6 and 7 experienced rewetting during accumulator injection at about 20 s followed by a reheating as shown in Figures 49 and 50. In the calculation, CHF only occurred up to Level 6 and the rewetting did not occur. In general, the agreement between measured and calculated clad temperature was best in the lower and middle core regions where the calculations of CHF predictions were consistent with measurement.

As discussed for Test S-28-1, the calculated thermal behavior of the four rods were not identical. Figure 52 shows the midcore calculated temperature responses of the four rods. The responses follow similar trends but variations of up to 100 K are observed. These differences were a result of small differences in fluid conditions among the four hydraulic cells at that elevation.

TABLE 11. MAXIMUM TEMPERATURE AS A FUNCTION OF CORE ELEVATION FOR TEST S-28-10

Core/Levels	Temperature (K)				
	Rod 1	Rod 2	Rod 3	Rod 4	Hot Rod
1 c ^a	713.1	704.9	703.1	701.5	710.8
m ^b	-- ^c	--	670.0	--	--
2 c	788.2	787.1	783.8	781.2	795.6
m	825.0	--	725.0	840.0	775.0
3 c	852.6	851.6	846.9	843.4	859.8
m	900.0	820.0	--	850.0	825.0
4 c	891.2	889.5	883.3	879.1	897.8
m	900.0	825.0	825.0	875.0	860.0

a. Calculated.

b. Measured.

c. No data available.

TABLE 12. COMPARISONS OF CALCULATED AND MEASURED CHF FOR TEST S-28-10

Core/Level	Hot Rod	Rod 1	Rod 2	Rod 3	Rod 4
1 c ^a	Y ^c	Y	Y	Y	Y
m ^b	Y	Y	Y	Y	Y
2 c	Y	Y	Y	Y	Y
m	Y	Y	Y	Y	Y
3 c	Y	Y	Y	Y	Y
m	Y	Y	Y	Y	Y
4 c	Y	Y	Y	Y	Y
m	Y	Y	Y	Y	Y
5 c	Y	Y	Y	Y	Y
m	Y	Y	Y	Y	Y
6 c	Y	Y	Y	Y	Y
m	-- ^d	Y	Y	Y	Y
7 c	N ^e	Y	N	N	N
m	--	Y	Y	Y	Y
8 c	N	N	N	N	N
m	--	Y	Y	--	Y
9 c	N	N	N	N	N
m	N	--	N	--	Y
10 c	N	N	N	N	N
m	N	--	N	N	--
11 c	N	N	N	N	N

a. Calculated.

b. Measured.

c. CHF occurrence.

d. No data.

e. No CHF.

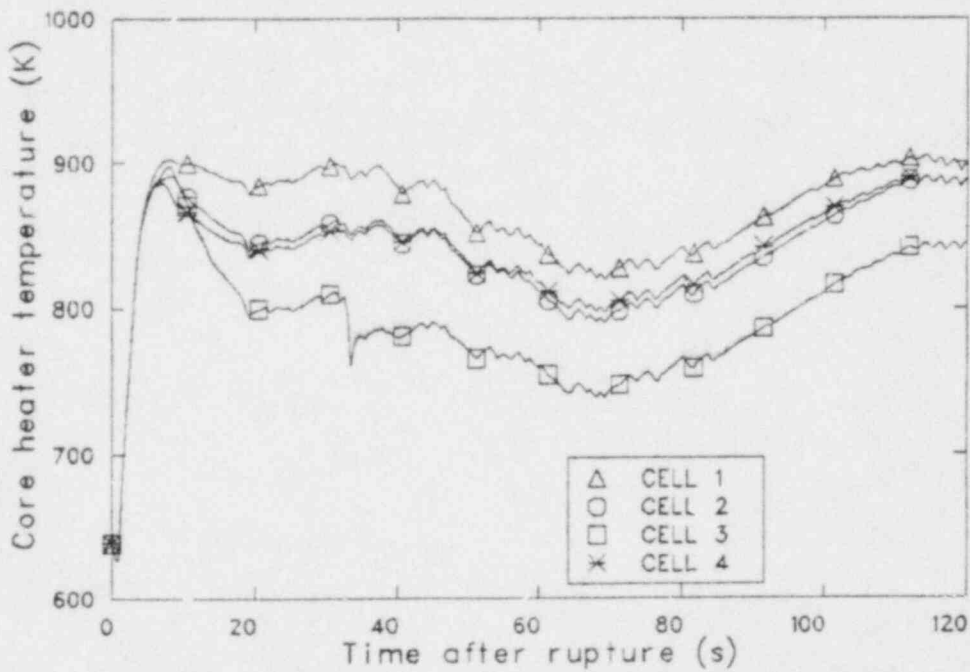


Figure 52. Calculated cladding temperatures of average core heater rods at mid core elevation for Test S-28-10.

5. USER EXPERIENCES

This section discusses problems encountered in using the TRAC-PD2 computer program and the approaches to resolve these problems.

5.1 Steady State Calculation

One advantage of TRAC code is that, in the steady state calculation, the user is not required to calculate the pressure and temperature distribution throughout the system. Instead, a representative hot leg and cold leg pressure and temperature can be used for the entire hot leg and cold leg components. The code will perform a calculation to provide a steady state system pressure and temperature distribution. However, it is common that this calculated steady state condition does not agree with the test initial conditions.

If the calculated system pressure and temperature do not agree with test data, the user can adjust either the steam generator secondary side pressure or the feedwater mass flow rate.

When the calculated cold leg temperature is higher than the data, the steam generator secondary side saturation temperature can be lowered by this difference. This new saturation temperature and its corresponding pressure are then used as new secondary side fluid conditions. Experience has shown that about 0.22 MPa decrease in secondary side pressure yielded better agreement on the system pressure and temperature.

5.2 Transient Calculation

All trip signals are set by the code during the initial transient calculation. In the subsequent restart calculations, these trip data are no longer required as input. In fact, the presence of trip data in the transient restart calculation will reset the trip initiation time back to zero which causes errors on those trip signals using time as reference parameter.

The accumulator and its associated check valve are another potential areas of calculational difficulty. The check valve is tripped open when system pressure drops to a value lower than accumulator pressure. After the initiation of accumulator discharge, there might be a time period during which system pressure fluctuations cause the check valve to be open and closed repeatedly. During this time period, the code might be required to use very small time steps and still have convergence failure. To bypass this problem, the valve can be changed to a valve which stays open until tripped to close.

Also, at the end of accumulator discharge there may be a small reverse flow from the system back to the accumulator. Since the accumulator is essentially empty at this time, the valve may be closed thereafter if convergence problems occur.

6. CONCLUSIONS AND RECOMMENDATIONS

Conclusions and recommendations resulting from this study were:

1. The capability of TRAC-PD2 to calculate the core temperature response was strongly dependent on its capability to calculate the occurrence of CHF.

In those core regions (lower and middle core) where CHF occurred in the experiment and was also calculated by the code, the temperature comparisons were significantly better than in the regions (upper core) where there were differences in CHF occurrences.

2. TRAC-PD2 capabilities to calculate the effects resulting from injecting hot secondary fluid into the hot leg were limited.

The amount of the injected liquid that was flashed to steam was overestimated in the calculation which resulted in less liquid flowing into the hot leg from the simulated tube ruptures. The smaller amount of liquid flowing from the hot leg into the upper core resulted in a smaller region of the core being quenched from the liquid from the steam generator.

3. The code is capable of simulating both the top and bottom quench observed in the experiment.

A top down quench from the rupture liquid in Test S-28-1 was predicted in the calculation. The bottom up quench from the reflooding process in Test S-28-10 was also predicted by the code.

5. In general, the code is capable of predicting the over-all trend of the system thermal-hydraulic response.

The TRAC-PD2 calculation shows the general trends of the system thermal-hydraulic parameters and the agreement is good in general.

6. Improvement is recommended in the steam generator model.

With the steam generator finely nodalized to include the downcomer and steam separator, a steady state could not be achieved without changing the boundary conditions of the feedwater mass flow. Review and improvement of the heat transfer methodology of this component is recommended.

7. REFERENCES

1. B. L. Collins, C. E. Coppin, K. E. Sackett, Experiment Data Report for Semiscale Mod-1, Test S-28-1, TREE-NUREG-1148, October 1977.
2. R. L. Gillins, V. Esparza, K. E. Sackett, C. E. Coppin, Experiment Data Report for Semiscale Mod-1 Test S-28-8, S-28-10, and S-28-11, TREE-NUREG-1155, March 1978.
3. E. M. Feldman and D. J. Olson, Semiscale Mod-1 Program and System Description for the Blowdown Heat Transfer Test (Test Series 2), ANCR-1230, August 1975.
4. J. M. Cozzuol, O. M. Hanner, G. G. Loomis, Investigation of the Influence of Simulated Steam Generator Tube Ruptures During Loss-of-Coolant Experiments in the Semiscale Mod-1 System, TREE-NUREG-1213, May 1978.
5. TRAC-PD2, An Advanced Best-Estimate Computer Program for Pressurized Water Reactor Loss-of-Coolant Accident Analysis Los Alamos National Laboratory (to be published).
6. P. N. Demmie, An Analysis of Semiscale Mod-1 LOCE S-04-6 Using the TRAC-PD2 Computer Program, EG-CAAP-5181, June 1980.
7. J. C. Vigil et al., TRAC-PIA Developmental Assessment, LA-8056-MS, October 1979.

APPENDIX A
ERROR ESTIMATES OF DATA IN TESTS S-28-1 and S-28-10

TABLE A-1. MEASUREMENTS AND THEIR UNCERTAINTIES

<u>Measurement</u>	<u>Detector Range</u>	<u>Measurement System Total Probable Error</u>
Fluid temperature	273 to 1533 K	<u>+3 K</u>
Rod temperature	273 to 1533 K	<u>+3 K</u>
Upper plenum pressure	0 to 20.7 MPa	<u>+1% full scale^a</u>
Accumulator volumetric flow rate	<u>+0.32 to +3.79</u> l/s	<u>+0.095 l/s</u>
Fluid density	0.16 to 1602 kg/m ³	<u>+16.0 kg/m³</u>

a. Detector full scale range.